

# Kitaev spin-orbital bilayers and their moiré superlattices

Emilian Nica<sup>1</sup>, Muhammad Akram<sup>1</sup>, Aayush Vijayvargia<sup>1</sup>, Roderich Moessner<sup>2</sup>, Onur Erten<sup>1</sup>

<sup>1</sup>*Department of Physics, Arizona State University, Tempe, AZ 85287, USA*

<sup>2</sup>*Max-Planck-Institut für Physik komplexer Systeme, Nöthnitzer Strasse 38, 01187 Dresden, Germany*

We determine the phase diagram of a bilayer, Kitaev spin-orbital model with inter-layer interactions ( $J$ ), for several stackings and moiré superlattices. For AA stacking, a gapped  $\mathbb{Z}_2$  quantum spin liquid phase emerges at a finite  $J_c$ . We show that this phase survives in the well-controlled large- $J$  limit, where an isotropic honeycomb toric code emerges. For moiré superlattices, a finite- $\mathbf{q}$  inter-layer hybridization is stabilized. This connects inequivalent Dirac points, effectively ‘untwisting’ the system. Our study thus provides insight into the spin-liquid phases of bilayer spin-orbital Kitaev materials.

Quantum spin liquids (QSLs) are disordered phases of magnetic systems with emergent exotic properties arising from their underlying topological character [1–5]. The Kitaev model on the honeycomb lattice [6, 7] is of particular significance as the first member of a family of exactly-solvable models, which exhibit both abelian and non-abelian QSL phases. Recent years have witnessed experimental progress in identifying candidate materials which include a number of iridates [8] and  $\alpha$ - $\text{RuCl}_3$  [9]. Apart from these, Kitaev interactions can also be strong in other van der Waals (vdW) materials such as  $\text{CrI}_3$  [10, 11]. Moreover, vdW materials can in principle be arranged in several stacking patterns and can be twisted to form moiré superlattices, potentially leading to new phases. Indeed, a number of recent theoretical studies [12–17] predict a variety of noncoplanar magnetic phases including skyrmions, in twisted vdW magnets, some of which have been realized experimentally [18, 19].

We study the zero-temperature phase diagram of bilayer versions of Kitaev spin-orbital models, initially proposed by Yao and Lee [20], with additional inter-layer Heisenberg spin-exchange interactions. Spin-orbital models are generalizations of the original Kitaev model with extra local orbital degrees of freedom (DOF) and Kugel-Khomskii interactions involving both spin and orbital sectors [21], [20, 22–30]. Much like Kitaev’s original proposal, spin and orbital DOF can each be represented in terms of three-flavored sets of Majorana fermions. The Yao-Lee model also exhibits an emergent  $\mathbb{Z}_2$  gauge symmetry with associated gapped flux excitations (visons), which are defined exclusively in terms of the orbital DOF [20]. The inter-layer spin-exchange interactions therefore commute with the intra-layer (orbital) flux operators, in contrast to general spin-exchange interactions in Kitaev’s original model and subsequent bilayer realizations [31–33]. We take advantage of this unique feature by considering only the lowest-energy, zero-flux sector, and by working in a gauge where all of the bonds are uniform and identical. Furthermore, we treat the spin-exchange interactions in the Hartree approximation. This introduces an effective inter-layer hybridization for

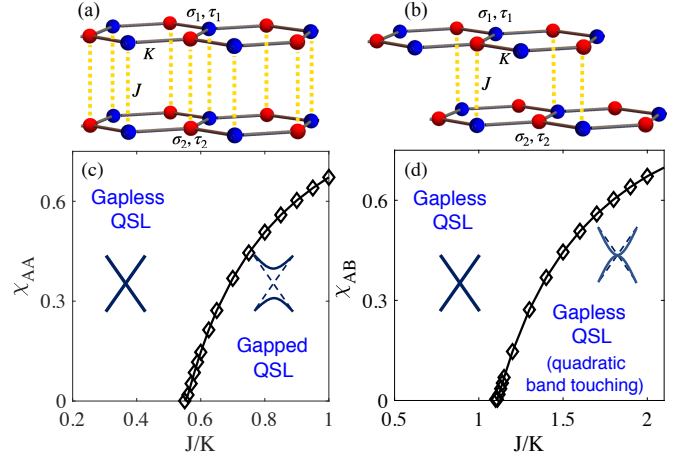


FIG. 1: Illustration of the Yao-Lee bilayer model for (a) AA and (b) AB stacking patterns.  $K$  and  $J$  are the intra-layer Kitaev and inter-layer Heisenberg spin exchange terms, respectively. (c) Effective inter-layer hybridization obtained via a Hartree approximation for AA stacking. A finite hybridization indicates the formation of inter-layer singlets and leads to gapped itinerant Majorana fermions. (d) Same for AB stacking. A finite hybridization leads to a phase with quadratic band touching for the Majorana fermions.

the itinerant Majorana fermions associated with the spin DOF. A non-zero expectation value indicates the formation of inter-layer spin-singlets, as shown in the Supplemental Material (SM).

We focus on AA stacking patterns and moiré superlattices, which exhibit fully-gapped spectra, but also briefly cover the gapless, AB stacking case. For AA stacking, the effective hybridization becomes non-zero at a finite value of the inter-layer exchange coupling, and opens a gap in the itinerant Majorana fermion spectrum. This signals a topological phase transition to a gapped  $\mathbb{Z}_2$  QSL. We support our Hartree approximation with two additional considerations. First, we show that the bilayer model is equivalent to an attractive Hubbard model with three flavors of complex fermions, for our choice of gauge. Previous studies beyond the Hartree approximation have shown that the Hubbard model exhibits a single transi-

tion to a charge density wave (CDW) phase [34], which is equivalent to the bilayer with a non-zero inter-layer hybridization. Secondly, we show that in the limit of large inter-layer spin-exchange interactions, the bilayer model maps onto Kitaev's toric code [35], which is gapped in both orbital and spin sectors, and which exhibits topological order. This naturally suggests that the gapped phase predicted by the Hartree approximation is adiabatically connected to the toric code, as the gaps in either spin or orbital sectors would otherwise close in the intermediate regime. For AB stacking, the formation of inter-layer spin singlets leaves the itinerant Majorana fermions gapless with quadratic band touching, in analogy with bilayer graphene [36]. For moiré superlattices, we consider both uniform ( $\mathbf{q} = 0$ ) and modulated inter-layer effective hybridizations ( $\mathbf{q} \neq 0$ ). In contrast to the  $\mathbf{q} = 0$  case, the finite- $\mathbf{q}$  hybridization connects inequivalent Dirac points in the moiré Brillouin Zone (BZ), effectively 'untwisting' the system, and opens a gap in the itinerant Majorana spectrum. In turn, this leads to the emergence of a gapped  $\mathbb{Z}_2$  QSL, as for AA stacking.

Kitaev spin-orbital models are likely to be realized in strongly spin-orbit coupled  $4d$  and  $5d$  Mott insulators, as predicted by a number of recent studies [26, 37–39]. For instance, an enhanced  $SU(4)$  symmetry [40] has been advanced for  $\alpha$ - $ZrCl_3$ . The unique signatures of the gapless QSL phase in monolayer Yao-Lee models, as probed by inelastic neutron scattering, have also been predicted recently [28].

*Model.* We consider two identical intra-layer Hamiltonians consisting of Yao-Lee[20] interactions on a honeycomb lattice,

$$H_\nu = \sum_{\alpha\text{-links}, \langle ij \rangle} K^{(\alpha)} \left( \tau_{\nu,i}^{(\alpha)} \tau_{\nu,j}^{(\alpha)} \right) (\boldsymbol{\sigma}_{\nu,i} \cdot \boldsymbol{\sigma}_{\nu,j}) \quad (1)$$

where  $K^{(\alpha)}$  is the nearest neighbor coupling constant for type- $\alpha$  links ( $\alpha \in \{x, y, z\}$ ) as shown in Fig 1 (a)-(b). The sites of the honeycomb lattice are labeled by the  $i$  and  $j$  indices, while  $\nu \in \{1, 2\}$  denotes the two layers. An exact solution is obtained by introducing Majorana fermion representations for the spin and orbital DOF in each layer:  $\sigma_{\nu,j}^{(\alpha)} = -i\epsilon^{\alpha\beta\gamma} c_{\nu,j}^{(\beta)} c_{\nu,j}^{(\gamma)}/2$  and  $\tau_{\nu,j}^{(\alpha)} = -i\epsilon^{\alpha\beta\gamma} d_{\nu,j}^{(\beta)} d_{\nu,j}^{(\gamma)}/2$  [20]. These representations are redundant and the physical states in each layer must be restricted to the eigenstates of  $D_{\nu,i} = -i c_{\nu,i}^{(x)} c_{\nu,i}^{(y)} c_{\nu,i}^{(z)} d_{\nu,i}^{(x)} d_{\nu,i}^{(y)} d_{\nu,i}^{(z)}$  operators with eigenvalues 1. As in Kitaev's original model, these constraints can be formally imposed via projection operators  $P_\nu = \prod_i (1 + D_{\nu,i})/2$ . The intra-layer Hamiltonians in the Majorana representation can be expressed as  $H_\nu = P_\nu \mathcal{H}_\nu P_\nu$ , where

$$\mathcal{H}_\nu = \sum_{\langle ij \rangle} K^{(\alpha)} u_{\nu,ij}^\alpha [i c_{\nu,i}^{(x)} c_{\nu,j}^{(x)} + i c_{\nu,i}^{(y)} c_{\nu,j}^{(y)} + i c_{\nu,i}^{(z)} c_{\nu,j}^{(z)}]. \quad (2)$$

The bond operators  $u_{\nu,ij}^{(\alpha)} = -i d_{\nu,i}^{(\alpha)} d_{\nu,j}^{(\alpha)}$ , commute with  $\mathcal{H}_\nu$ , and are therefore conserved with eigenvalues  $\pm 1$ . The  $SO(3)$  spin rotation symmetry is reflected by the presence of three flavors of itinerant Majorana fermions. Both  $\mathcal{H}_\nu$  are invariant under separate  $\mathbb{Z}_2$  gauge transformations  $c_{\nu,i}^{(\alpha)} \rightarrow -c_{\nu,i}^{(\alpha)}$ ;  $u_{ij}^{(\alpha)} \rightarrow -u_{ij}^{(\alpha)}$  with flux operators which are defined by the product of the  $u_{ij}^{(\alpha)}$  around hexagonal plaquettes.

Lieb's theorem [41] predicts that the ground state lies in the zero-flux sector, with a finite vison gap. We can thus obtain the itinerant Majorana spectrum by choosing a gauge where  $u_{ij} = 1 \forall \langle ij \rangle$  in both layers. Unless otherwise stated, we will use this choice throughout. The three decoupled flavors of itinerant Majorana fermions have identical spectra which can be determined via a Fourier transform defined on half of the BZ of the honeycomb lattice [20]. The spectra are gapless for  $K_x + K_y > K_z$  and gapped otherwise. Here, we consider the symmetric, gapless case with  $K_x = K_y = K_z = K$ .

In contrast to Kitaev's original proposal, the Yao-Lee model, which describes each of the two layers, involves flux excitations (visons) which are defined exclusively in terms of the orbital DOF, while the itinerant Majorana excitations stem from the spin DOF alone. Consequently, any additional terms involving the spin DOF only, including a bilayer coupling, commute with the flux operator. The resulting spectrum can *a priori* preserve the gapped flux excitations, in contrast to the original Kitaev model [31–33]. Guided by this important aspect, we consider Yao-Lee bilayers coupled via inter-layer antiferromagnetic Heisenberg interactions  $H_I = \sum_{ij} J_{ij} \boldsymbol{\sigma}_{1i} \cdot \boldsymbol{\sigma}_{2j}$ , where (1, 2) are layer indices, and where we allow for general  $J_{ij}$  coupling beyond nearest-neighbors (NN). The bilayer Hamiltonian in the Majorana representation is  $\mathcal{H} = \sum_\nu \mathcal{H}_\nu + \mathcal{H}_I$  where

$$\mathcal{H}_I = \sum_{i,j;\alpha \neq \beta} \frac{J_{ij}}{2} \left( c_{1i}^{(\alpha)} c_{2j}^{(\alpha)} c_{1i}^{(\beta)} c_{2j}^{(\beta)} \right). \quad (3)$$

*Self-consistent solutions for AA and AB stacking patterns.* In contrast to the intra-layer terms, the inter-layer interactions are bi-quadratic in the itinerant Majorana operators, thus precluding a closed-form solution. Instead, we treat the inter-layer interactions within a Hartree approximation. This approach is backed up by additional considerations, as discussed further below.

For the purpose of illustration, we restrict the inter-layer coupling to NN pairs. We do not expect that weaker couplings beyond NNs will qualitatively alter our conclusions. The interaction term in eq. 3 can be decoupled in Hartree and magnetic channels [42]. We are interested in zero-temperature solutions which stabilize QSL phases and consider on-site order parameters in the Hartree channel  $\langle \chi_i^{(\alpha)} \rangle = \langle i c_{1i}^{(\alpha)} c_{2i}^{(\alpha)} \rangle$ , which preserve the  $SO(3)$  spin symmetry. We consequently drop the corresponding flavor indices. As shown in the SM, a non-zero

$\langle \chi \rangle$  marks the formation of inter-layer spin singlets. A  $\mathbb{Z}_2$  gauge transformation involving site  $i$  flips the signs of the  $u_{ij}$  bonds emanating from  $i$  in the same layer, while also changing the sign of the inter-layer  $\langle \chi \rangle$  on the same site. Consequently,  $\langle \chi_i \rangle$  is not gauge invariant since it is only defined up to a sign.

For the AA stacking pattern, the A and B sublattice sites overlap, as shown in Fig. 1 (a). The inter-layer interactions involve two pairs of sites per unit cell:  $\mathcal{H}_I = -2J[\sum_{i \in A, \alpha} \langle \chi_{AA} \rangle (ic_{1i}^\alpha c_{2i}^\alpha) + \sum_{j \in B, \alpha} \langle \chi_{BB} \rangle (ic_{1j}^\alpha c_{2j}^\alpha)]$ . Solutions which are both uniform and symmetric in the sublattice index ( $\chi_{AA} = \chi_{BB}$ ) amount to gapless itinerant Majorana fermions, with shifted Dirac cones, as for AA-stacked bilayer graphene. In contrast, when the hybridization has an alternating sign on the two sublattices ( $\langle \chi_{AA} \rangle = -\langle \chi_{BB} \rangle$ ), the itinerant Majorana spectrum is gapped, leading to a lower ground state energy. Our self-consistent solutions are shown in Fig. 1 (c) as functions of  $J/K$ . We find that the critical value for this transition is  $J_c/K = 0.55$ .

To establish the stability of our solutions beyond the Hartree approximation, we map  $\mathcal{H}$  to an equivalent form by using complex fermions involving linear combinations of Majorana fermions on overlapping sites  $f_i^\alpha = (c_{1i}^\alpha + ic_{2i}^\alpha)/2$ :

$$\mathcal{H} = 2K \sum_{\langle ij \rangle, \alpha} (if_{A,i}^\alpha f_{B,j}^\alpha + \text{H.c.}) - 2J \sum_i \left( n_i - \frac{3}{2} \right)^2 \quad (4)$$

where  $n_i = \sum_\alpha f_i^{\alpha\dagger} f_i^\alpha$ . For  $J > 0$ , eq. 4 describes an attractive Hubbard model with three flavors of complex fermions. This model exhibits a single, broken-symmetry CDW phase with finite  $\langle n_A - n_B \rangle$ , as determined by quantum Monte Carlo simulations [34]. The CDW order parameter is equivalent to the alternating-sign  $\chi$  solutions of the Yao-Lee bilayer. Note that the equivalence holds for the choice of gauge considered here. While the CDW breaks inversion symmetry in the Hubbard model, the same cannot be said of the effective hybridization in the bilayer model, since the former is not gauge invariant. Nevertheless, the effective hybridization cannot be made to vanish in any gauge, and the resulting phases are always gapped.

For an AB stacking pattern, the A sublattice sites of layer 1 lie directly on top of the B sublattice sites of layer 2, with a single bond per unit cell, as shown in Fig. 1 (b). As a result, for finite  $\chi$  beyond  $J_c/K \simeq 1.1$ , the itinerant Majorana spectrum is similar to that of AB-stacked bilayer graphene with quadratic band touching [36]. The self-consistent solutions for  $\langle \chi_{AB} \rangle$  are shown in Fig. 1 (d). A mapping to an equivalent model as in the AA case is not apparent here.

We expect that all of our results survive the projection onto the physical Hilbert space. As shown in the SM for AA stacking, the projection operator  $P$  acting on the ground state ansatz symmetrizes the latter over all

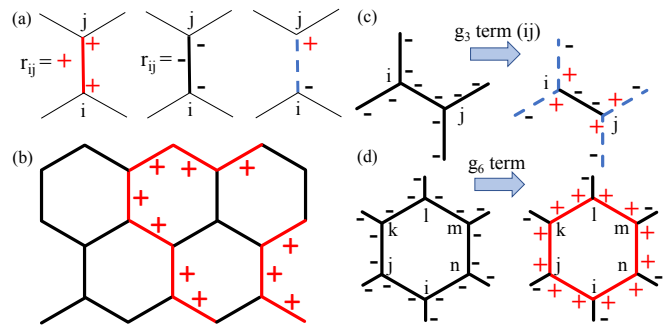


FIG. 2: (a) The bond operator  $r_{ij}$ . Red (blue) lines correspond to + (-) bonds.  $r_{ij}$  is not defined for blue dashed lines. (b) A state in the ground state manifold which minimizes the  $g_2$  terms and which also obeys the local product constraint, leading to bonds obeying an Ising Gauss's law. (c)  $g_3$  terms on sites  $i, j$  flip four adjacent bonds. (d)  $g_6$  terms flip the plaquette bond configurations.

bond and  $\langle \chi_i \rangle$  configurations which are consistent with a zero flux. While the set of  $\langle \chi_i \rangle$  are zero for these gauge-symmetrized states, we can define a gauge-invariant correlator, whose expectation value in the projected ground-state is consistent with  $\langle \chi_{AA} \rangle = -\langle \chi_{BB} \rangle$ .

*Limit of large inter-layer interactions with AA stacking pattern.* Next, we consider the AA stacking pattern in the limit of large, NN inter-layer ( $J$ ) terms. To zeroth order in the intra-layer ( $K$ ) terms, the model describes a collection of independent inter-layer spin singlets with degenerate orbital states. We derive an effective Hamiltonian perturbatively up to 6<sup>th</sup> order in  $K/J$

$$H_{\text{eff}} = \sum_{\substack{\alpha\text{-links} \\ \langle ij \rangle}} \left( g_2 \tau_{1i}^{(\alpha)} \tau_{2i}^{(\alpha)} \tau_{1j}^{(\alpha)} \tau_{2j}^{(\alpha)} + g_3 \sum_{\nu=1,2} \tau_{\nu i}^{(\alpha)} \tau_{\nu j}^{(\alpha)} \right) + g_6 \sum_{\square, \nu} W_p^\nu \quad (5)$$

where  $W_p^{1(2)}$  is the flux operator defined on the honeycomb plaquettes on layer 1(2) as  $W_p^\nu = \tau_{\nu i}^{(z)} \tau_{\nu j}^{(y)} \tau_{\nu k}^{(x)} \tau_{\nu l}^{(z)} \tau_{\nu m}^{(y)} \tau_{\nu n}^{(x)}$  (Fig. 2 (d)). Please consult the SM for additional details. The coupling constants are  $g_2 = -K^2/4J$ ,  $g_3 = -K^3/J^2$ , and  $g_6 = -K^6/(8J)^5$ . The  $g_2$  term describes Kitaev interactions around *inter-layer plaquettes* while the  $g_3$  term is a standard Kitaev interaction in each layer. We first focus on the the leading  $g_2$  terms. It is convenient to define new operators  $p_i^{(\alpha)} = \tau_{i1}^{(\alpha)} \tau_{2i}^{(\alpha)}$ , which unlike the  $\tau$ 's, all commute with each other. Furthermore their product amounts to  $p_i^{(x)} p_i^{(y)} p_i^{(z)} = -1$ . Therefore, we use local basis states which are eigenstates of all  $p$  operators and which also satisfy the product rule:  $\{|-, -, -\rangle, |-, +, +\rangle, |+, -, +\rangle, |+, +, -\rangle\}$  where  $\pm$  denotes the eigenvalue of  $p^{(\alpha)}$ , ( $\alpha = x, y, z$ ). The first of these is an inter-layer (orbital) singlet while the remain-

ing are triplet states. The  $g_2 < 0$  terms favor equal- $\alpha$  states on NN sites. Therefore, for bond configurations that minimize the  $g_2$  terms, it is possible to define bond variables  $r_{ij} = \pm 1$  for pairs of  $(+, +)$  and  $(-, -)$  eigenvalues of  $p_{i/j}^{(\alpha)}$ , respectively. For bond configurations that do not minimize the  $g_2$  terms,  $r_{ij}$  is not defined. Fig. 2 (a) illustrates this construction. In addition to having bond configurations which minimize the  $g_2$  terms, the ground state manifold must also satisfy the local constraint due to  $p_i^{(x)} p_i^{(y)} p_i^{(z)} = -1$ . Taken together, these conditions are equivalent to bond configurations which obey an Ising Gauss's law  $G_i^P = \prod_{\gamma} r_{ij} = -1$ , as illustrated in Fig. 2 (b).

Next, we examine the effect of  $g_3$  and  $g_6$  terms acting on the ground state manifold obtained from the combined effects of the  $g_2$  terms and local product constraints. Each  $\tau_{1,2}^{(\alpha)}$  acting on  $|p_x, p_y, p_z\rangle$  preserves the corresponding  $\alpha$  eigenvalues but flips the remaining two, up to an overall phase (see SM). Therefore, the  $g_6$  terms acting on a plaquette flips all of the  $r_{ij}$  bond variables therein (Fig 2 (d)), leading to an effective term

$$-\kappa \sum_{\square} (|\circ\rangle\langle\bar{\circ}| + \text{H.c.}) \quad (6)$$

In contrast, the single  $g_3$  term on sites  $\langle ij \rangle$ , connects a ground-state configuration to excited states, see Fig. 2 (c). Consecutive application of  $g_3$  terms around a plaquette leads to plaquette flips, but these processes are subdominant with respect to those due to the  $g_6$  term.

The resonance term in eq. 6, along with Gauss' law, describe Kitaev's toric code [35] on a honeycomb lattice. We thus conclude that the bilayer model in the limit of large inter-layer spin exchange interactions is in a gapped abelian  $\mathbb{Z}_2$  topological QSL phase.

*Self-consistent solutions for moiré superlattices.* We generalize the Hartree approximation to include the effects of small-angle twists. We follow the approach in Ref. 43 to derive a low-energy theory defined on the usual moiré extended BZ, for details see the SM.

To allow for non-vanishing inter-layer interactions under arbitrary, small twist angles, we extend the former beyond overlapping NN pairs with an implicit decay with increasing pair separation. In general, this implies a non-trivial dependence of the coupling constant on crystal momentum, and also allows for interactions which are delocalized in the extended BZ. In the low-energy limit, the interactions are limited to the vicinity of a set of equivalent crystal momenta throughout the extended BZ. Instead on focusing on a particular realization of such finite-range interactions, we only consider states in the vicinity of a finite set of crystal momenta, chosen to explicitly preserve a minimal  $C_3$  rotation symmetry. For simplicity, we set all couplings to be equal. We also limit the hybridization to states in the vicinity of Dirac points in neighboring moiré reciprocal unit cells. This trun-

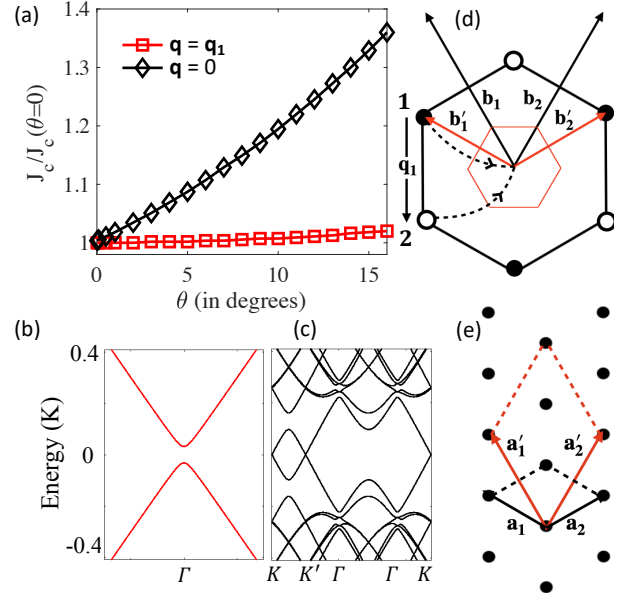


FIG. 3: Moiré superlattices: (a) critical inter-layer exchange ( $J_c$ ) as a function of twisting angle  $\theta$  for  $\mathbf{q} = 0$  and  $\mathbf{q} = \mathbf{q}_1$ . The itinerant Majorana fermion spectrum for (b)  $\mathbf{q} = \mathbf{q}_1$  and (c)  $\mathbf{q} = 0$ . (d) The moiré lattice vectors (black) for  $J < J_c$  and  $J > J_c$  (red) corresponding to the finite- $\mathbf{q}$  solution. (e) Moiré reciprocal unit cells as in (d). 1 and 2 denote the Dirac points of the two layers which are separated by a  $\theta$ -dependent  $\mathbf{q}_1$  in the absence of a finite inter-layer hybridization. When the latter acquires a finite value for  $J > J_c$ , the two Dirac points are shifted to the  $\Gamma$  point of the folded BZ, and are subsequently gapped.

cation is justified in the low-energy limit, where small-momentum scattering processes are dominant. These approximations ensure that the form of the effective hybridization bears a close resemblance to that of twisted bilayer graphene [43], as shown below.

In the low-energy limit, the intra-layer terms amount to the usual Dirac fermions for the two layers, which are shifted with respect to each other due to twisting in the extended moiré BZ. The inter-layer interactions in this limit, together with the approximations discussed previously can be written as

$$\mathcal{H}_I = -\frac{4J}{N} \sum_{nm} \left[ \langle \chi_{00}^\dagger(\mathbf{q}) \rangle \chi_{nm}(\mathbf{q}) + \langle \chi_{00}(\mathbf{q}) \rangle \chi_{nm}(-\mathbf{q}) \right] + \text{H.c.} \quad (7)$$

where

$$\chi_{nm}(\mathbf{q}) = i \sum_{\mathbf{k}} \left[ c_{1,\alpha;nm}^{\dagger,(\mu)}(\mathbf{k}) c_{2,\beta;nm}^{(\mu)}(\mathbf{k} - \mathbf{q}) + e^{-i\mathbf{g}_2 \cdot (\boldsymbol{\tau}_\alpha - \boldsymbol{\tau}_\beta)} c_{1,\alpha;nm}^{\dagger,(\mu)}(\mathbf{k}) c_{2,\beta;n+1m}^{(\mu)}(\mathbf{k} - \mathbf{q}) + e^{-i\mathbf{g}_3 \cdot (\boldsymbol{\tau}_\alpha - \boldsymbol{\tau}_\beta)} c_{1,\alpha;nm}^{\dagger,(\mu)}(\mathbf{k}) c_{2,\beta;nm+1}^{(\mu)}(\mathbf{k} - \mathbf{q}) \right] \quad (8)$$

and

$$c_{\alpha,1/2}^{\dagger,(\mu)}(\mathbf{K}_{00} + \mathbf{k} - n\mathbf{b}_2 - m\mathbf{b}_3) = c_{\alpha,1/2;nm}^{\dagger,(\mu)}(\mathbf{k}) \quad (9)$$

are states with an effective Dirac dispersion which is shifted by the moiré reciprocal vectors  $\mathbf{b}_{2,3}$  with respect to the Dirac point centered on the moiré first BZ at  $n = m = 0$ .  $\mathbf{K}_{00}$  is the position of the Dirac point of layer 1 in the first BZ, which plays no role in the effective low-energy theory but is included here for consistency, while  $\mathcal{G}_{2,3}$  are the reciprocal unit vectors of layer 1. The sums over momenta  $\mathbf{k}$  cover the extended moiré BZ, with an implicit cutoff. The vectors  $\boldsymbol{\tau}_{\alpha,\beta}$  denote the shift of the A, B sublattices in layers 1 and 2, respectively.  $\mathbf{q}$  is a vector contained within a single moiré reciprocal unit cell.

We consider two cases, one for  $\mathbf{q} = 0$  corresponding to a uniform effective inter-layer hybridization, and another for finite  $\mathbf{q} = \mathbf{q}_1$  where  $\mathbf{q}_1 = -8\pi/3 \sin(\theta/2)\hat{y}$  [43] which denotes the shift between the Dirac points in layers 1 and 2 in the first BZ due to twisting (see Fig. 3 (e)). In both cases,  $\langle \chi_{AA} \rangle = -\langle \chi_{BB} \rangle$  acquire finite expectation values whereas  $\langle \chi_{AB} \rangle$  and  $\langle \chi_{BA} \rangle$  remain pinned to zero. Our self-consistent calculations indicate that the critical coupling  $J_c/K$  for the  $\mathbf{q} = \mathbf{q}_1$  solution is below its  $\mathbf{q} = 0$  counterpart for the entire range of twist angles considered here (Fig. 3 (a)), indicating that the modulated hybridization is energetically favored. A finite- $\mathbf{q}$  hybridization connects states near inequivalent Dirac points in the moiré BZ and gaps the spectrum, as illustrated in Fig. 3 (b), effectively ‘untwisting’ the system. In contrast, for  $\mathbf{q} = 0$ , the low-energy spectrum remains gapless, as shown in Fig. 3 (c). Consequently, the finite- $\mathbf{q}$  solution is preferred for any non-zero twist angle. The two solutions merge smoothly as  $\theta \rightarrow 0$  since  $\mathbf{q}_1$ , at which point the low-energy sectors match the self-consistent solutions of the un-twisted bilayer with AA stacking.

For the gauge choice of uniform and identical bonds in both layers, the  $\mathbf{q} = \mathbf{q}_1$  incommensurate, inter-layer hybridization breaks the translation symmetry of simple moiré pattern but preserves all other symmetries. It consequently triples the size of the moiré unit cell (Fig. 3 (d)). Fig. 3 (e) shows the moiré (black) and folded (red) BZ’s, respectively. The rotated Dirac cones at the corners of the moiré BZ are folded onto the  $\Gamma$  point. However, since the effective hybridization is not gauge invariant, this does not imply a true translation symmetry breaking in the bilayer, but instead demonstrates that small-angle twisting preserves the gap in the itinerant Majorana spectrum, and that the gapped  $\mathbb{Z}_2$  QSL for AA stacking remains stable at zero temperature.

*Discussion.* It is instructive to compare the Yao-Lee and Kitaev bilayers with similar inter-layer spin exchange interactions. In the latter case, a mean-field study predicts gapped QSL and trivial dimer phases for intermediate and large values of the inter-layer coupling, respectively [31]. However, an exact diagonalization study [32]

finds that a single phase transition between gapless QSL and trivial dimer phases occurs at a substantially weaker critical coupling  $J/K \sim 0.06$ . Our results indicate that the QSL phase remains stable in Yao-Lee bilayers for large but finite intra-layer couplings, while the trivial dimer phase emerges only in the absence of intra-layer terms ( $K = 0$ ). We attribute the stability of the gapped QSL in our case to inter-layer spin exchange interactions which preserve the flux sectors of both layers. Moiré superlattices of Kitaev bilayers were addressed in Ref. 33 in the highly anisotropic toric code limit with strong local interactions.

*Conclusion.* We studied the zero-temperature phase diagram of a bilayer Yao-Lee model with inter-layer spin-exchange interactions in the Hartree approximation for several stacking patterns and moiré superlattices. For AA stacking, we determined that finite inter-layer singlet correlations gap the itinerant Majorana fermion spectrum. This conclusion was supported by an exact mapping to an attractive Hubbard model, which similarly shows a single transition. We also derived an effective Hamiltonian in the limit of large, inter-layer interactions to several leading orders in the intra-layer coupling, and demonstrated that it maps onto the toric code. In the absence of any additional transitions which close the gap, we concluded that the solutions obtained via the Hartree approximation are adiabatically connected to the large inter-layer interaction limit, leading to the stability of a topological gapped  $\mathbb{Z}_2$  QSL. This phase persists for moiré superlattices under small-angle twisting. For AB stacking, the Majorana fermions remain gapless. Our results suggest that spin-orbital Kitaev bilayers can in general be tuned to gapped  $\mathbb{Z}_2$  QSL phases for sufficiently strong inter-layer spin exchange interactions. Detailed studies of the AB stacked phases and of the toric code models in the large inter-layer coupling limit are clearly desirable.

We thank Piers Coleman and Filip Ronning for fruitful discussions. OE acknowledge support from NSF Award No. DMR 1904716. MA is supported by Fulbright Scholarship. This work was in part supported by the Deutsche Forschungsgemeinschaft under grants SFB 1143 (project-id 247310070) and the cluster of excellence ct.qmat (EXC 2147, project-id 390858490). We acknowledge the ASU Research Computing Center for HPC resources.

- 
- [1] L. Balents, Nature **464**, 199 (2010), URL <https://doi.org/10.1038/nature08917>.
  - [2] Y. Zhou, K. Kanoda, and T.-K. Ng, Rev. Mod. Phys. **89**, 025003 (2017), URL <https://link.aps.org/doi/10.1103/RevModPhys.89.025003>.
  - [3] X.-G. Wen, Rev. Mod. Phys. **89**, 041004 (2017), URL <https://link.aps.org/doi/10.1103/RevModPhys.89.041004>.
  - [4] J. Knolle and R. Moessner, Annual Review of Condensed

- Matter Physics **10**, 451 (2019), URL <https://doi.org/10.1146/annurev-conmatphys-031218-013401>.
- [5] C. Broholm, R. J. Cava, S. A. Kivelson, D. G. Nocera, M. R. Norman, and T. Senthil, *Science* **367**, eaay0668 (2020), URL <https://www.science.org/doi/abs/10.1126/science.aay0668>.
- [6] A. Kitaev, *Annals of Physics* **321**, 2 (2006), URL <https://www.sciencedirect.com/science/article/pii/S0003491605002381>.
- [7] M. Hermanns, I. Kimchi, and J. Knolle, *Annual Review of Condensed Matter Physics* **9**, 17 (2018), <https://doi.org/10.1146/annurev-conmatphys-033117-053934>, URL <https://doi.org/10.1146/annurev-conmatphys-033117-053934>.
- [8] S. Hwan Chun, J.-W. Kim, J. Kim, H. Zheng, C. C. Stoumpos, C. D. Malliakas, J. F. Mitchell, K. Mehlawat, Y. Singh, Y. Choi, et al., *Nature Physics* **11**, 462 (2015), URL <https://doi.org/10.1038/nphys3322>.
- [9] H. Takagi, T. Takayama, G. Jackeli, G. Khaliullin, and S. E. Nagler, *Nature Reviews Physics* **1**, 264 (2019), URL <https://doi.org/10.1038/s42254-019-0038-2>.
- [10] I. Lee, F. G. Utermohlen, D. Weber, K. Hwang, C. Zhang, J. van Tol, J. E. Goldberger, N. Trivedi, and P. C. Hammel, *Phys. Rev. Lett.* **124**, 017201 (2020), URL <https://link.aps.org/doi/10.1103/PhysRevLett.124.017201>.
- [11] M. Blei, J. L. Lado, Q. Song, D. Dey, O. Erten, V. Pardo, R. Comin, S. Tongay, and A. S. Botana, *Applied Physics Reviews* **8**, 021301 (2021), URL <https://doi.org/10.1063/5.0025658>.
- [12] Q. Tong, F. Liu, J. Xiao, and W. Yao, *Nano Letters* **18**, 7194 (2018), URL <https://doi.org/10.1021/acs.nanolett.8b03315>.
- [13] K. Hejazi, Z.-X. Luo, and L. Balents, *Proceedings of the National Academy of Sciences* **117**, 10721 (2020), URL <https://www.pnas.org/content/117/20/10721>.
- [14] K. Hejazi, Z.-X. Luo, and L. Balents, *Phys. Rev. B* **104**, L100406 (2021), URL <https://link.aps.org/doi/10.1103/PhysRevB.104.L100406>.
- [15] M. Akram and O. Erten, *Phys. Rev. B* **103**, L140406 (2021), URL <https://link.aps.org/doi/10.1103/PhysRevB.103.L140406>.
- [16] F. Xiao, K. Chen, and Q. Tong, *Phys. Rev. Research* **3**, 013027 (2021), URL <https://link.aps.org/doi/10.1103/PhysRevResearch.3.013027>.
- [17] M. Akram, H. LaBollita, D. Dey, J. Kapeghian, O. Erten, and A. S. Botana, *Nano Letters* **21**, 6633 (2021), URL <https://doi.org/10.1021/acs.nanolett.1c02096>.
- [18] Y. Xu, A. Ray, Y.-T. Shao, S. Jiang, K. Lee, D. Weber, J. E. Goldberger, K. Watanabe, T. Taniguchi, D. A. Muller, et al., *Nature Nanotechnology* (2021), URL <https://doi.org/10.1038/s41565-021-01014-y>.
- [19] T. Song, Q.-C. Sun, E. Anderson, C. Wang, J. Qian, T. Taniguchi, K. Watanabe, M. A. McGuire, R. Stöhr, D. Xiao, et al., *Science* **374**, 1140 (2021), URL <https://www.science.org/doi/abs/10.1126/science.abj7478>.
- [20] H. Yao and D.-H. Lee, *Phys. Rev. Lett.* **107**, 087205 (2011), URL <https://link.aps.org/doi/10.1103/PhysRevLett.107.087205>.
- [21] K. I. Kugel and D. I. Khomskii, **25**, 231 (1982), URL <https://doi.org/10.1070/pu1982v025n04abeh004537>.
- [22] H. Yao, S.-C. Zhang, and S. A. Kivelson, *Phys. Rev. Lett.* **102**, 217202 (2009), URL <https://link.aps.org/doi/10.1103/PhysRevLett.102.217202>.
- [23] F. Wang and A. Vishwanath, *Phys. Rev. B* **80**, 064413 (2009), URL <https://link.aps.org/doi/10.1103/PhysRevB.80.064413>.
- [24] C. Wu, D. Arovas, and H.-H. Hung, *Phys. Rev. B* **79**, 134427 (2009), URL <https://link.aps.org/doi/10.1103/PhysRevB.79.134427>.
- [25] V. S. de Carvalho, H. Freire, E. Miranda, and R. G. Pereira, *Phys. Rev. B* **98**, 155105 (2018), URL <https://link.aps.org/doi/10.1103/PhysRevB.98.155105>.
- [26] U. F. P. Seifert, X.-Y. Dong, S. Chulliparambil, M. Vojta, H.-H. Tu, and L. Janssen, *Phys. Rev. Lett.* **125**, 257202 (2020), URL <https://link.aps.org/doi/10.1103/PhysRevLett.125.257202>.
- [27] S. Chulliparambil, U. F. P. Seifert, M. Vojta, L. Janssen, and H.-H. Tu, *Phys. Rev. B* **102**, 201111 (2020), URL <https://link.aps.org/doi/10.1103/PhysRevB.102.201111>.
- [28] W. M. H. Natori and J. Knolle, *Phys. Rev. Lett.* **125**, 067201 (2020), URL <https://link.aps.org/doi/10.1103/PhysRevLett.125.067201>.
- [29] S. Chulliparambil, L. Janssen, M. Vojta, H.-H. Tu, and U. F. P. Seifert, *Phys. Rev. B* **103**, 075144 (2021), URL <https://link.aps.org/doi/10.1103/PhysRevB.103.075144>.
- [30] A. M. Tsvelik and P. Coleman, arXiv:2112.07781 (2021), URL <https://arxiv.org/abs/2112.07781>.
- [31] U. F. P. Seifert, J. Gritsch, E. Wagner, D. G. Joshi, W. Brenig, M. Vojta, and K. P. Schmidt, *Phys. Rev. B* **98**, 155101 (2018), URL <https://link.aps.org/doi/10.1103/PhysRevB.98.155101>.
- [32] H. Tomishige, J. Nasu, and A. Koga, *Phys. Rev. B* **99**, 174424 (2019), URL <https://link.aps.org/doi/10.1103/PhysRevB.99.174424>.
- [33] J. May-Mann and T. L. Hughes, *Phys. Rev. B* **101**, 245126 (2020), URL <https://link.aps.org/doi/10.1103/PhysRevB.101.245126>.
- [34] H. Xu, Z. Zhou, X. Wang, L. Wang, and Y. Wang, arXiv:1912.11233 (2019), URL <https://arxiv.org/abs/1912.11233>.
- [35] A. Kitaev, *Annals of Physics* **303**, 2 (2003), URL <https://www.sciencedirect.com/science/article/pii/S0003491602000180>.
- [36] A. Rozhkov, A. Sboychakov, A. Rakhmanov, and F. Nori, *Physics Reports* **648**, 1 (2016), electronic properties of graphene-based bilayer systems, URL <https://www.sciencedirect.com/science/article/pii/S0370157316301612>.
- [37] W. M. H. Natori, R. Nutakki, R. G. Pereira, and E. C. Andrade, *Phys. Rev. B* **100**, 205131 (2019), URL <https://link.aps.org/doi/10.1103/PhysRevB.100.205131>.
- [38] C. Xu, J. Feng, M. Kawamura, Y. Yamaji, Y. Nahas, S. Prokhorenko, Y. Qi, H. Xiang, and L. Bellaiche, *Phys. Rev. Lett.* **124**, 087205 (2020), URL <https://link.aps.org/doi/10.1103/PhysRevLett.124.087205>.
- [39] P. P. Stavropoulos, D. Pereira, and H.-Y. Kee, *Phys. Rev. Lett.* **123**, 037203 (2019), URL <https://link.aps.org/doi/10.1103/PhysRevLett.123.037203>.
- [40] M. G. Yamada, M. Oshikawa, and G. Jackeli, *Phys. Rev. Lett.* **121**, 097201 (2018), URL <https://link.aps.org/doi/10.1103/PhysRevLett.121.097201>.
- [41] E. H. Lieb, *Phys. Rev. Lett.* **73**, 2158 (1994), URL <https://link.aps.org/doi/10.1103/PhysRevLett.73.2158>.
- [42] B. S. Shastry and D. Sen, *Phys. Rev. B* **55**,

2988 (1997), URL <https://link.aps.org/doi/10.1103/PhysRevB.55.2988>.

- [43] R. Bistritzer and A. H. MacDonald, Proceedings of the National Academy of Sciences **108**, 12233 (2011), URL <https://www.pnas.org/content/108/30/12233>.

# Supplemental Materials for “Kitaev spin-orbital bilayers and their moiré superlattices”

Emilian Nica<sup>1</sup>, Muhammad Akram<sup>1</sup>, Aayush Vijayvargia<sup>1</sup>, Roderich Moessner<sup>2</sup>, Onur Erten<sup>1</sup>

<sup>1</sup>*Department of Physics, Arizona State University, Tempe, AZ 85287, USA*

<sup>2</sup>*Max-Planck-Institut für Physik Komplexer Systeme,  
Nöthnitzer Strasse 38, 01187 Dresden, Germany*

## I. INTER-LAYER SINGLETS IN THE MAJORANA REPRESENTATION

In the main text, we remark that a finite effective hybridization indicates the formation of static inter-layer singlet pairs. A similar connection has been discussed in previous works, which employed an exact Majorana representation of the spin operators [S1, S2]. We summarize these arguments here.

We introduce an equivalent basis of complex fermions by taking linear combinations of two itinerant Majorana fermions of the same flavor on overlapping sites in the two layers:

$$f_i^{(\alpha)} = \frac{1}{2} \left( c_{1i}^{(\alpha)} + i c_{2i}^{(\alpha)} \right). \quad (\text{S1})$$

The corresponding Fock space is determined by the three occupation numbers  $n_i^{(\alpha)} = f_i^{\dagger,(\alpha)} f_i^{(\alpha)}$ , where  $\alpha \in \{x, y, z\}$ .

To illustrate the connection between the Fock states and the Hilbert space of the local spins, we consider the inter-layer coupling for a single pair of overlapping sites:

$$H_{I,j} = J \boldsymbol{\sigma}_{1j} \cdot \boldsymbol{\sigma}_{2j} \quad (\text{S2})$$

For antiferromagnetic interactions, this has a inter-layer singlet ground state and three excited triplet states at  $4J$ . When expressed in terms of the complex fermions,  $H_{I,j}$  becomes

$$H_{I,j} = -2J \left( \sum_{\alpha} n_j^{(\alpha)} - \frac{3}{2} \right)^2 \quad (\text{S3})$$

For  $J > 0$ , there are two degenerate ground-state configurations with  $n_j^{(x)} = n_j^{(y)} = n_j^{(z)}$  equal to 0 and 1, respectively, and six degenerate excited states at  $4J$  for the remaining configurations. The Fock states thus provide two redundant representations of the product space of the two spins, which can be distinguished by the fermion parity  $\prod_{\alpha} (2n_j^{(\alpha)} - 1)$ . The connection can also be made explicit by matching the matrix elements of the spin operators in either basis [S1, S2],

In the complex fermion representation, the effective hybridization becomes

$$\begin{aligned} \langle \chi_j^{(\alpha)} \rangle &= \langle i c_{1j}^{(\alpha)} c_{2j}^{(\alpha)} \rangle \\ &= \left( 2n_j^{(\alpha)} - 1 \right). \end{aligned} \quad (\text{S4})$$

For the degenerate spin-singlet ground state sector of even and odd fermion parities,  $\langle \chi_j^{(x)} \rangle = \langle \chi_j^{(y)} \rangle = \langle \chi_j^{(z)} \rangle = \pm 1$ , respectively. This statement can be generalized beyond a single pair of spins. For  $J > 0$ , a local hybridization which is non-zero and equal for all three flavors indicates the presence of inter-layer singlets in the ground-state.

In our calculations, the redundancy of the Majorana or complex fermion representations for pairs of spins was explicitly removed by choosing a gauge where all of the bond variables are equal to 1.

## II. PROJECTION ONTO PHYSICAL SPACE

In the main text, we state that the expectation value of a gauge-invariant correlator in a state obtained by projecting our fixed-gauge ansatz onto the physical sector is consistent with a finite effective hybridization, for AA stacking. Here, we show that this is the case.



### A. Effect of projection operator

We denote our ground state ansatz with a set of finite  $\langle \chi_i \rangle$  in a fixed gauge with uniform bonds equal to 1 by

$$|\Psi\rangle = |\forall u_{1,ij} = 1\rangle \otimes |\forall u_{2,ij} = 1\rangle \otimes |\langle \chi_{AA} \rangle = -\langle \chi_{BB} \rangle\rangle. \quad (\text{S5})$$

for  $i, j \in \{1, 2, \dots, N\}$ , where  $N$  is the number of sites. We chose periodic boundary conditions for both layers and assumed an even number of unit cells  $N_c = N/2$ . In the trivially dimerized limit for  $J \neq 0, K = 0$   $|\Psi\rangle$  can be labeled by the eigenvalues of all  $\chi_i$  operators. In this case, states obtained by flipping at least one of the  $\langle \chi_i \rangle$ 's are orthogonal to  $|\Psi\rangle$ . In the following, we assume that this can be generalized to ansätze where the  $\chi_i$ 's are not individually conserved for  $K \neq 0$ .

We consider the operators

$$D_{\nu,i} = -i c_{\nu,i}^{(x)} c_{\nu,i}^{(y)} c_{\nu,i}^{(z)} d_{\nu,i}^{(x)} d_{\nu,i}^{(y)} d_{\nu,i}^{(z)}, \quad (\text{S6})$$

where  $\nu$  is a layer index, acting on  $|\Psi\rangle$ .  $D_{\nu,i}$  anti-commutes with the bond operators  $u_{\nu,ij}^{(\alpha)} = -i d_{\nu,i}^{(\alpha)} d_{\nu,j}^{(\alpha)}$  in layer  $\nu$  and with  $\chi_i^{(\alpha)}$  for all three  $\alpha$  flavors. Its effect on  $|\Psi\rangle$  amounts to a  $\mathbb{Z}_2$  gauge transformation which flips the three bonds emanating from site  $i$  in layer  $\nu$  and  $\langle \chi_i \rangle$  for all flavors on the same site. Any two  $D$  operators commute and obey  $D_{\nu,i}^2 = 1$ .

The projection operator  $P$  is given by

$$P = 2^{-2N} \left[ \prod_{i=1}^N \left( \frac{1 + D_{1,i}}{2} \right) \right] \left[ \prod_{i=1}^N \left( \frac{1 + D_{2,i}}{2} \right) \right]. \quad (\text{S7})$$

For each layer, the product of  $D_{\nu,i}$  operators over any subset of sites  $\Lambda$  differs from that over the complementary set by the product over all sites:

$$\prod_{i \in \Lambda} D_{\nu,i} = \left( \prod_{j \notin \Lambda} D_{\nu,j} \right) \left( \prod_{k=1}^N D_{\nu,k} \right). \quad (\text{S8})$$

We can also express the projection operator as [S3]

$$P = 2^{-2N} \prod_{\nu} \left[ \left( \sum'_{\{i\}} \prod_{i \in \{i\}} D_{\nu,i} \right) \left( 1 + \prod_{i=1}^N D_{\nu,i} \right) \right] \quad (\text{S9})$$

where the primed summations, involving products of at most  $N/2$  operators, cover half of all possible combinations, and thus include  $2^{N-1}$  separate realizations. The terms in the second parentheses can be expressed as

$$\left( 1 + \prod_{i=1}^N D_i^{(1)} \right) \left( 1 + \prod_{j=1}^N D_j^{(2)} \right) = 2 \left( 1 + \prod_{i=1}^N D_i^{(1)} \right) \left( \frac{1 + P_0}{2} \right) \quad (\text{S10})$$

where

$$P_0 = \prod_{i=1}^N D_{1,i} D_{2,i} \quad (\text{S11})$$

since

$$\prod_{i=1}^N D_{2,i} = \prod_{i=1}^N D_{1,i} P_0. \quad (\text{S12})$$

The projection operator can therefore be written as

$$P = 2^{-2N+1} \left( \sum'_{\{i\}} \prod_{i \in \{i\}} D_{1,i} \right) \left( \sum'_{\{j\}} \prod_{j \in \{j\}} D_{2,j} \right) \left( 1 + \prod_{i=1}^N D_{1,i} \right) \left( \frac{1 + P_0}{2} \right) \quad (\text{S13})$$

The effect of  $P_0$  acting on  $|\Psi\rangle$  is discussed further below. Of the remaining terms, the first parenthesis denotes a sum over all products of at most  $N/2$  operators, each of which flips bond operators in layer 1 and the corresponding  $\langle\chi_i\rangle$ . The terms in the second parenthesis do the same in layer 2. The non-trivial part of the third parenthesis leaves all of the bond variables in both layers invariant, but flips all  $\langle\chi_i\rangle$ . The resulting non-trivial states differ from  $|\Psi\rangle$  by at least three bonds in either layer or by a finite set of  $\langle\chi_i\rangle$ , and are therefore orthogonal by assumption.

We now consider  $P_0$ , which can be re-cast as

$$P_0 = \prod_{l=1}^{N_c} D_{1,lA} D_{1,lB} D_{2,lA} D_{2,lB} = (-1)^{N_c} \left[ \prod_l \prod_\alpha (id_{lA}^{1\alpha} d_{lB}^{1\alpha}) \right] \left[ \prod_l \prod_\alpha (id_{lA}^{2\alpha} d_{lB}^{2\alpha}) \right] \left[ \prod_l \prod_\alpha (2n_{f,lA}^{(\alpha)} - 1) (2n_{f,lB}^{(\alpha)} - 1) \right] \quad (\text{S14})$$

where A and B denote the two sublattices and where we used the relation between  $\chi_i$  and the local complex fermion parity introduced in Eq. S4. The  $l$  indices label the  $N_c$  unit cells. The terms in the first two brackets correspond to the total fermion parities of the  $\mathbb{Z}_2$  gauge fields on layers 1 and 2, respectively [S4]. The remaining terms determine the total parity of the itinerant fermions:

$$\left[ \prod_l \prod_\alpha (2n_{f,lA}^{(\alpha)} - 1) (2n_{f,lB}^{(\alpha)} - 1) \right] = (-1)^{\sum_l \sum_\alpha (n_{f,lA}^{(\alpha)} + n_{f,lB}^{(\alpha)})}. \quad (\text{S15})$$

The itinerant fermion parity thus depends on the total filling.

As mentioned previously, we consider periodic boundary conditions along with an even number of unit cells along each of the two directions of the Bravais lattice. The fermion parities of the  $\mathbb{Z}_2$  gauge fields are then both even [S4]. Since the itinerant (complex) fermion sector is in a charge density wave phase at half filling, the fermion parity associated with these states is simply  $(-1)^{3N_c}$ . Consequently, the effect of  $P_0$  on  $|\Psi\rangle$  is trivial

$$\left( \frac{1 + P_0}{2} \right) |\Psi\rangle = |\Psi\rangle. \quad (\text{S16})$$

This implies that  $P$  acting on  $|\Psi\rangle$  is

$$P |\Psi\rangle = 2^{-2N+1} \left( \sum_{\{i\}} \prod_{i \in \{i\}} D_i^{(1)} \right) \left( \sum_{\{j\}} \prod_{j \in \{j\}} D_j^{(2)} \right) \left( 1 + \prod_i D_i^{(1)} \right) |\Psi\rangle. \quad (\text{S17})$$

Note that the resulting state involves a linear combination over  $2^{2N-1}$  distinct configurations.

## B. Gauge-invariant correlator

We can define a gauge-invariant operator [S5, S6]

$$C_{ij}^{(\alpha)} = \left( \prod_{\alpha\text{-links}, \langle i'j' \rangle} u_{1,i'j'}^{(\alpha)} \right) \left( \prod_{\alpha\text{-links}, \langle i''j'' \rangle} u_{2,i''j''}^{(\alpha)} \right) \chi_{iA}^{(\alpha)} \chi_{jB}^{(\alpha)} \quad (\text{S18})$$

where  $\prod'$  and  $\prod''$  denote products of  $u$  bonds in the upper and lower layer, respectively, which connect the two sites  $i, j$  on A and B sublattices, respectively. For convenience, we choose overlapping paths in both layers. For the case of preserved  $\text{SO}(3)$  symmetry considered here, we drop the flavor indices. The expectation value of  $C_{ij}$  is the same in any state  $|\Psi'\rangle$  which is gauge equivalent to  $|\Psi\rangle$ . This is because  $D_{\nu,k}$  either flips two bonds in the product of  $u$ 's in layer  $\nu$  for  $k \neq i, j$ , or flips one bond and inverts  $\langle\chi_i\rangle$  for  $k \in \{i, j\}$ , respectively. This operator is also invariant under gauge transformations which do not change any of the bonds but which flip all  $\langle\chi_i\rangle$ .  $C_{ij}$  also preserves all of the bond variables. Therefore, we can write

$$\langle\Psi'|C_{ij}|\Psi'\rangle = \langle\Psi|\chi_{iA}\chi_{jB}|\Psi\rangle \quad (\text{S19})$$

together with

$$\lim_{|\mathbf{R}_i - \mathbf{R}_j| \rightarrow \infty} \langle \Psi' | C_{ij} | \Psi' \rangle \approx \langle \Psi | \chi_A | \Psi \rangle \langle \Psi | \chi_B | \Psi \rangle. \quad (\text{S20})$$

as the itinerant Majorana spectrum is gapped in this case. A finite  $C_{ij}$  in any gauge and in the limit of asymptotically large separation is equivalent to a non-zero order parameter in our choice of gauge.

We now determine the effect of the projector on the expectation values of  $C_{ij}$ . As shown previously,  $P$  acting on  $|\Psi\rangle$  generates a linear combination involving  $2^{2N-1}$  distinct states. This implies that

$$\begin{aligned} \langle \Psi | P^2 | \Psi \rangle &= (2^{-4N+2}) (2^{2N-1}) \\ &= 2^{-2N+1} \end{aligned} \quad (\text{S21})$$

where the two terms on the first line are due to the overall powers of  $1/2$  and to the number of distinct configurations, respectively. Since  $C_{ij}$  does not connect any two distinct configurations we obtain

$$\begin{aligned} \frac{\langle \Psi | P C_{ij} P | \Psi \rangle}{\langle \Psi | P^2 | \Psi \rangle} &= \frac{2^{-2N+1} \langle \Psi | C_{ij} | \Psi \rangle}{2^{-2N+1}} \\ &= \langle \Psi | \chi_{iA} \chi_{jB} | \Psi \rangle \end{aligned} \quad (\text{S22})$$

Therefore, the expectation value of the gauge-invariant correlator in a projected ground state ansatz is consistent with the effective hybridization obtained in a fixed gauge without any additional projection. Our conclusions survive the projection to the physical space.

### III. DERIVATION OF THE EFFECTIVE HAMILTONIAN

In this section, we provide the details of the derivation of the effective Hamiltonian in the large inter-layer exchange limit. We start with two singlets formed between layer 1 and 2 on sites  $i$  and  $j$ , that are connected via an  $\alpha$  ( $\alpha = x, y, z$ ) bond. The unperturbed states are  $|\phi\rangle = |S, \tau\rangle_i |S, \tau\rangle_j$  where  $|S\rangle = |\uparrow_1 \downarrow_2 - \downarrow_1 \uparrow_2\rangle$  is the singlet state and 1 and 2 are the layer subindices.  $|\tau\rangle$  is the orbital component of the wave function. For  $K = 0$ , the orbital sector is degenerate as there is no term in the Hamiltonian that couples to the  $\tau$ 's. We perturb the degenerate manifold of  $|\phi\rangle$  with the  $K$  term that couples the two singlets

$$H_K = K [\tau_{1i}^\alpha \tau_{1j}^\alpha (\sigma_{1i} \cdot \sigma_{1j}) + \tau_{2i}^\alpha \tau_{2j}^\alpha (\sigma_{2i} \cdot \sigma_{2j})] \quad (\text{S23})$$

The first order correction to the energy vanishes  $E^{(1)} = \langle \phi | H_K | \phi \rangle = 0$ . The second order correction to the energy is

$$\begin{aligned} E^{(2)} &= \frac{\sum_{m \neq \phi} |\langle m | H_K | \phi \rangle|^2}{E_\phi - E_m} \\ &= -\frac{K^2}{2J}, \quad \text{for } \langle \tau_{1i}^\alpha \tau_{2i}^\alpha \tau_{1j}^\alpha \tau_{2j}^\alpha \rangle = 1 \\ &= 0, \quad \text{for } \langle \tau_{1i}^\alpha \tau_{2i}^\alpha \tau_{1j}^\alpha \tau_{2j}^\alpha \rangle = -1 \end{aligned} \quad (\text{S24})$$

where  $\langle \tau_{1i}^\alpha \tau_{2i}^\alpha \tau_{1j}^\alpha \tau_{2j}^\alpha \rangle$  is the eigenvalue of the inter-layer plaquette operator evaluated in the degenerate  $|\phi\rangle$  manifold. This leads to the second order term in the effective Hamiltonian,  $g_2 \tau_{1i}^\alpha \tau_{2i}^\alpha \tau_{1j}^\alpha \tau_{2j}^\alpha$  where  $g_2 = -K^2/4J$ . The third order correction to the energy is

$$\begin{aligned} E^{(3)} &= \sum_{m \neq \phi, n \neq \phi} \frac{\langle \phi | H_K | m \rangle \langle m | H_K | n \rangle \langle n | H_K | \phi \rangle}{(E_\phi - E_m)(E_\phi - E_n)} \\ &= -\frac{K^3}{J^2} (\langle \tau_{1i}^\alpha \tau_{1j}^\alpha \rangle + \langle \tau_{2i}^\alpha \tau_{2j}^\alpha \rangle) \end{aligned} \quad (\text{S25})$$

which gives rise to the  $g_3(\tau_{1i}^\alpha \tau_{1j}^\alpha + \tau_{2i}^\alpha \tau_{2j}^\alpha)$  term with  $g_3 = -K^3/J^2$ . Apart from the pairwise interactions, we also consider a ring-exchange term around a honeycomb. The unperturbed states are the six singlet states with degenerate orbital wave functions:  $|\phi\rangle = |S, \tau\rangle_i |S, \tau\rangle_j |S, \tau\rangle_k |S, \tau\rangle_l |S, \tau\rangle_m |S, \tau\rangle_n$  (see Fig. 2(d) in the main text). The sixth order correction to the energy that involves the ring exchange gives

$$E^{(6)} = +\frac{K^6}{J^5} (\langle \tau_{1i}^x \tau_{1j}^x \tau_{1j}^z \tau_{1k}^z \tau_{1k}^y \tau_{1l}^y \tau_{1l}^x \tau_{1m}^x \tau_{1m}^z \tau_{1n}^z \tau_{1n}^y \tau_{1i}^y + \tau_{2i}^x \tau_{2j}^x \tau_{2j}^z \tau_{2k}^z \tau_{2k}^y \tau_{2l}^y \tau_{2l}^x \tau_{2m}^x \tau_{2m}^z \tau_{2n}^z \tau_{2n}^y \tau_{2i}^y \rangle) \quad (\text{S26})$$

$$= -\frac{K^6}{(8J)^5} (\langle W_p^1 + W_p^2 \rangle) \quad (\text{S27})$$

where  $W_p^{1(2)} = \tau_{1(2)i}^z \tau_{1(2)j}^y \tau_{1(2)k}^x \tau_{1(2)l}^z \tau_{1(2)m}^y \tau_{1(2)n}^x$  is the flux operator for layer 1(2). Therefore the ring-exchange term is  $g_6(W_p^1 + W_p^2)$  with  $g_6 = -K^6/(8J)^5$ .

#### IV. PROJECTING THE THIRD ORDER TERM ONTO THE GROUND STATE MANIFOLD

As discussed in the main text, the eigenstates of the  $g_2$  terms in the effective Hamiltonian are given in terms of the states  $|p^x, p^y, p^z\rangle$  where  $p^\alpha = \pm$  is the eigenvalue of the  $p^\alpha = \tau_1^\alpha \tau_2^\alpha$  operator. The ground state of  $g_2$  term also need to satisfy the Ising Gauss law:  $G_i^P = \prod_\gamma r_{ij} = -1$  where  $r_{ij} = \pm 1$  for pairs of  $(+, +)$  and  $(-, -)$  eigenvalues of  $p_{i/j}^{(\alpha)}$ , respectively. However  $|p^x, p^y, p^z\rangle$  states are not eigenstates of the  $g_3$  and  $g_6$  terms. Below, we present the matrix elements of  $\tau_{1,2}^\alpha$  operators on the  $|p^x, p^y, p^z\rangle$  states.

$$\begin{aligned}
\tau_1^x |-, -, -\rangle &= -|-, +, +\rangle \\
\tau_2^x |-, -, -\rangle &= +|-, +, +\rangle \\
\tau_1^y |-, -, -\rangle &= i|+, -, +\rangle \\
\tau_2^y |-, -, -\rangle &= -i|+, -, +\rangle \\
\tau_1^z |-, -, -\rangle &= +|+, +, -\rangle \\
\tau_2^z |-, -, -\rangle &= -|+, +, -\rangle \\
\tau_1^x |-, +, +\rangle &= -|-, -, -\rangle \\
\tau_2^x |-, +, +\rangle &= +|-, -, -\rangle \\
\tau_1^y |-, +, +\rangle &= i|+, +, -\rangle \\
\tau_2^y |-, +, +\rangle &= i|+, +, -\rangle \\
\tau_1^z |-, +, +\rangle &= +|+, -, +\rangle \\
\tau_2^z |-, +, +\rangle &= +|+, -, +\rangle \\
\tau_1^x |+, -, +\rangle &= +|+, +, -\rangle \\
\tau_2^x |+, -, +\rangle &= +|+, +, -\rangle \\
\tau_1^y |+, -, +\rangle &= -i|-, -, -\rangle \\
\tau_2^y |+, -, +\rangle &= +i|-, -, -\rangle \\
\tau_1^z |+, -, +\rangle &= +|-, +, +\rangle \\
\tau_2^z |+, -, +\rangle &= +|-, +, +\rangle \\
\tau_1^x |+, +, -\rangle &= +|+, -, +\rangle \\
\tau_2^x |+, +, -\rangle &= +|+, -, +\rangle \\
\tau_1^y |+, +, -\rangle &= -i|-, +, +\rangle \\
\tau_2^y |+, +, -\rangle &= -i|-, +, +\rangle \\
\tau_1^z |+, +, -\rangle &= +|-, -, -\rangle \\
\tau_2^z |+, +, -\rangle &= +|-, -, -\rangle
\end{aligned} \tag{S28}$$

We can summarize these matrix elements as follows:  $\tau_{1(2)}^{x(y,z)}$  acting on  $|p^x, p^y, p^z\rangle$  keeps the  $x(y, z)$  eigenvalue the same while flipping the other two eigenvalues. Therefore the  $g_6$  term acting on a plaquette flips the bond configuration, which gives rise to a term

$$-\kappa \sum_{\diamond} (|\diamond\rangle \langle \bar{\diamond}| + \text{H.c.}) \tag{S29}$$

where  $\diamond$  and  $\bar{\diamond}$  are conjugate  $p$  configurations around the hexagon. However,  $g_3$  acting on a bond that obeys the Gauss's law breaks 4 bonds, which takes it outside the ground state manifold. These virtual excitations can couple different ground state configurations when  $g_3$  term is applied around closed loops. The smallest loop is around a single honeycomb and when  $g_3$  term applied around a honeycomb also lead to flipping the bond configuration as in eq. S29. Since  $\kappa \sim g_3^6/g_2^5$ , it arises at  $K^8/J^7$  order in perturbation theory.

## V. EFFECTIVE HYBRIDIZATION FOR MOIRÉ SUPERLATTICES

In this section, we derive the mean-field Hamiltonian in the low-energy limit. For clarity, we shall use an expanded vector notation for the site indices. Our starting point is the interacting Hamiltonian

$$\mathcal{H} = \mathcal{H}_1 + \mathcal{H}_2 + \mathcal{H}_I, \quad (\text{S30})$$

where  $\mathcal{H}_{1,2}$  consist of intra-layer terms for the respective layers, while  $\mathcal{H}_I$  corresponds to the inter-layer interactions. Explicitly, these are

$$\begin{aligned} \mathcal{H}_1 &= \sum_{\mu} \sum_{\mathbf{R}} \sum_{\mathbf{l}} iK u_1(\mathbf{R}, \mathbf{l}) c_{A,1}^{(\mu)}(\mathbf{R}) c_{B,1}^{(\mu)}(\mathbf{R} + \mathbf{l}) \\ \mathcal{H}_2 &= \sum_{\mu} \sum_{\mathbf{R}'} \sum_{\mathbf{l}'} iK u_2(\mathbf{R}', \mathbf{l}') c_{A,2}^{(\mu)}(\mathbf{R}') c_{B,2}^{(\mu)}(\mathbf{R}' + \mathbf{l}') \end{aligned} \quad (\text{S31})$$

where  $\mathbf{R}, \mathbf{R}'$  are general Bravais lattice vectors of layer 1 and 2, respectively, while  $\mathbf{l}, \mathbf{l}'$  are Bravais lattice vector corresponding to the three nearest-neighbor (NN) unit cells. In all subsequent sections, un-primed and primed vectors correspond to vectors in layers 1 and 2, respectively. Furthermore, all real-space vectors are determined w.r.t. the intersection of the twist axis with the respective planes.  $\mu \in \{x, y, z\}$  stands for the flavor indices associated with both spin and orbital degrees-of-freedom (DOF). A and B are sublattice indices corresponding to

$$c_{A,1}^{(\mu)}(\mathbf{R}) = c_1^{(\mu)}(\mathbf{R} + \boldsymbol{\tau}_A) \quad (\text{S32})$$

$$c_{B,1}^{(\mu)}(\mathbf{R}) = c_1^{(\mu)}(\mathbf{R} + \boldsymbol{\tau}_B) \quad (\text{S33})$$

and similarly for layer 2. Note that the  $\boldsymbol{\tau}$ 's depend on the stacking pattern.

$$u_1(\mathbf{R}, \mathbf{l}) = -i d_{A,1}^{(\mu)}(\mathbf{R}) d_{B,1}^{(\mu)}(\mathbf{R} + \mathbf{l}) \quad (\text{S34})$$

are the bond operators [S7] consisting of two  $d$  Majorana operators used in the representation of the local orbital DOF. We use the same convention in defining the sublattice indices as for the itinerant  $c$  Majorana operators. We choose a gauge where the bond operators are independent of the flavor indices, and consequently drop the latter from all subsequent expressions.

The inter-layer spin-exchange interactions are

$$H_I = \frac{1}{2} \sum_{\mu \neq \nu} \sum_{\alpha, \beta} \sum_{\mathbf{R}, \mathbf{R}'} J(\mathbf{R} + \boldsymbol{\tau}_{\alpha} - \mathbf{R}' - \boldsymbol{\tau}'_{\beta}) c_{\alpha,1}^{(\mu)}(\mathbf{R}) c_{\alpha,1}^{(\nu)}(\mathbf{R}) c_{\beta,2}^{(\mu)}(\mathbf{R}') c_{\beta,2}^{(\nu)}(\mathbf{R}'). \quad (\text{S35})$$

The itinerant Majorana fermions obey

$$c_{\alpha,1}^{\dagger,(\mu)}(\mathbf{R}) = c_{\alpha,1}^{(\mu)}(\mathbf{R}) \quad (\text{S36})$$

together with

$$\{c_{\alpha,1}^{(\mu)}(\mathbf{R}), c_{\beta,1}^{(\nu)}(\mathbf{R}')\} = 2\delta_{\mathbf{R}, \mathbf{R}'} \delta_{\mu, \nu} \delta_{\alpha, \beta}, \quad (\text{S37})$$

and similarly for layer 2.

We next consider the expansion of the  $c$  Majorana fermions in terms of Bloch waves. Tilde momenta in the two layers are measured w.r.t. the intersections of the planes with the twist axis. Momenta without tilde are defined only in the vicinity of Dirac points in either layers, and are assumed to include a large number of moiré reciprocal unit cells for the small twist angles considered here. Finally, un-primed momenta correspond to layer 1, while primed momenta denote the layer 2 counterparts. With these conventions, we write

$$\begin{aligned} c_{\alpha,1}^{(\mu)}(\mathbf{R}) &= \frac{\sqrt{2}}{\sqrt{N}} \sum_{\tilde{\mathbf{k}} \in C/2} \left[ e^{-i\tilde{\mathbf{k}} \cdot (\mathbf{R} + \boldsymbol{\tau}_{\alpha})} c_{\alpha,1}^{(\mu)}(\tilde{\mathbf{k}}) + e^{i\tilde{\mathbf{k}} \cdot (\mathbf{R} + \boldsymbol{\tau}_{\alpha})} c_{\alpha,1}^{\dagger,(\mu)}(\tilde{\mathbf{k}}) \right] \\ c_{\alpha,2}^{(\nu)}(\mathbf{R}') &= \frac{\sqrt{2}}{\sqrt{N}} \sum_{\tilde{\mathbf{k}}' \in C'/2} \left[ e^{-i\tilde{\mathbf{k}}' \cdot (\mathbf{R}' + \boldsymbol{\tau}'_{\alpha})} c_{\alpha,2}^{(\nu)}(\tilde{\mathbf{k}}') + e^{i\tilde{\mathbf{k}}' \cdot (\mathbf{R}' + \boldsymbol{\tau}'_{\alpha})} c_{\alpha,2}^{\dagger,(\nu)}(\tilde{\mathbf{k}}') \right], \end{aligned} \quad (\text{S38})$$

where  $\alpha, \beta$  are sublattice indices, and  $N$  is the number of unit cells, assumed identical in either layer. The Majorana nature implies that [S4]

$$c_{\alpha,1}^{(\mu),\dagger}(\tilde{\mathbf{k}}) = c_{\alpha,1}^{(\mu)}(-\tilde{\mathbf{k}}) \quad (\text{S39})$$

where  $\mathbf{G}$  is a reciprocal vector. This redundancy is accounted for in Eqs. S38 by restricting the sums to one half of the primitive reciprocal unit cell, as shown in Fig. S1. The operators defined on  $C/2$  ( $C'/2$ ) obey the standard anti-commutation relations

$$\{c_{\alpha,1}^{\dagger,(\mu)}(\tilde{\mathbf{k}}_1), c_{\beta,1}^{(\nu)}(\tilde{\mathbf{k}}_2)\} = \delta_{\tilde{\mathbf{k}}_1, \tilde{\mathbf{k}}_2} \delta_{\mu, \nu} \delta_{\alpha, \beta}. \quad (\text{S40})$$

We assume periodic boundary conditions consistent with the uniform gauge choice adopted throughout the remaining sections, which imply the Bloch periodicity

$$e^{-i\mathbf{G}\cdot\boldsymbol{\tau}_\alpha} c_{\alpha,1}^{\dagger,(\mu)}(\tilde{\mathbf{k}}) = c_{\alpha,1}^{\dagger,(\mu)}(\tilde{\mathbf{k}} + \mathbf{G}), \quad (\text{S41})$$

and similarly for layer 2, where  $\mathbf{G}$  is a reciprocal lattice vector. In the following, it will prove convenient to extend the summations in Eq. S38 to  $N_c$  (half) reciprocal unit cells in the extended Brillouin Zone (BZ). Although such a procedure is redundant, it illustrates the emerging moiré periodicity in the low-energy limit.

### A. Intra-layer terms in the low-energy limit

We work in a gauge where both  $u_{1,2}$  are uniform and equal to 1. The intra-layer terms are

$$\mathcal{H}_1 = \frac{1}{N_c} \sum_{\mu} \sum_{\tilde{\mathbf{k}}} 2iK f_1(\tilde{\mathbf{k}}) c_{A,1}^{\dagger,(\mu)}(\tilde{\mathbf{k}}) c_{B,1}^{(\mu)}(\tilde{\mathbf{k}}) + \text{H.c.} \quad (\text{S42})$$

$$\mathcal{H}_2 = \frac{1}{N_c} \sum_{\mu} \sum_{\tilde{\mathbf{k}}'} 2iK f_2(\tilde{\mathbf{k}}') c_{A,2}^{\dagger,(\mu)}(\tilde{\mathbf{k}}') c_{B,2}^{(\mu)}(\tilde{\mathbf{k}}') + \text{H.c.} \quad (\text{S43})$$

where the momenta sums cover an extended BZ of half  $N_c$  primitive cells.

$$f_1(\tilde{\mathbf{k}}) = \sum_{\mathbf{l}} e^{i\tilde{\mathbf{k}}\cdot(\boldsymbol{\tau}_A - \boldsymbol{\tau}_B - \mathbf{l})} \quad (\text{S44})$$

$$f_2(\tilde{\mathbf{k}}') = \sum_{\mathbf{l}'} e^{i\tilde{\mathbf{k}}'\cdot(\boldsymbol{\tau}'_A - \boldsymbol{\tau}'_B - \mathbf{l}')} \quad (\text{S45})$$

are the familiar graphene form factors, with  $\mathbf{l}$  as defined previously. Note that these obey

$$f_1(\tilde{\mathbf{k}} + \mathbf{G}) e^{-i\mathbf{G}\cdot(\boldsymbol{\tau}_A - \boldsymbol{\tau}_B)} = f_1(\tilde{\mathbf{k}}). \quad (\text{S46})$$

and similarly for  $f_2$ .

We now proceed to take the low-energy limits of  $\mathcal{H}_{1,2}$ . Due to twisting, the Dirac points are shifted to

$$\mathbf{K}_{nm} = \mathbf{K}_{00} + n\boldsymbol{\mathcal{G}}_2 + m\boldsymbol{\mathcal{G}}_3 \quad (\text{S47})$$

$$\mathbf{K}'_{nm} = \mathbf{K}'_{00} + n\boldsymbol{\mathcal{G}}'_2 + m\boldsymbol{\mathcal{G}}'_3 \quad (\text{S48})$$

for layers 1 and 2, respectively. The  $n, m$  indices label the reciprocal unit cell translated from the first BZ at  $n = m = 0$  by a reciprocal lattice vector

$$\mathbf{G} = n\boldsymbol{\mathcal{G}}_2 + m\boldsymbol{\mathcal{G}}_3, \quad (\text{S49})$$

and similarly for layer 2. We expand the functions  $f_{1,2}$  for a common set of momenta

$$\tilde{\mathbf{k}} = \mathbf{K}_{00} + n\boldsymbol{\mathcal{G}}_2 + m\boldsymbol{\mathcal{G}}_3 + \mathbf{k} \quad (\text{S50})$$

with  $\mathbf{k}$  restricted to be in the vicinity of the Dirac points. Using the Bloch periodicity, we obtain

$$H_1 = \sum_{\mu} \sum_{\mathbf{k}} 2iK [\mathbf{k} \cdot \boldsymbol{\nabla} f_1(\mathbf{K}_{00})] c_{A,1}^{\dagger,(\mu)}(\mathbf{K}_{00} + \mathbf{k}) c_{B,1}^{(\mu)}(\mathbf{K}_{00} + \mathbf{k}) + \text{H.c.} \quad (\text{S51})$$

Since  $\mathbf{k}$  covers a large number of reciprocal moiré primitive unit cells, we can trivially extend the expression above to include shifted Dirac points as

$$H_1 = \frac{1}{N_c} \sum_{\mu} \sum_{n,m} \sum_{\mathbf{k}} 2iK [(\mathbf{k} - n\mathbf{b}_2 - m\mathbf{b}_3) \cdot \nabla f_1(\mathbf{K}_{00})] c_{A,1}^{\dagger,(\mu)}(\mathbf{K}_{00} + \mathbf{k} - n\mathbf{b}_2 - m\mathbf{b}_3) c_{B,1}^{(\mu)}(\mathbf{K}_{00} + \mathbf{k} - n\mathbf{b}_2 - m\mathbf{b}_3) + \text{H.c.} \quad (\text{S52})$$

where

$$\mathbf{b}_2 = \mathcal{G}'_2 - \mathcal{G}_2 \quad (\text{S53})$$

$$\mathbf{b}_3 = \mathcal{G}'_3 - \mathcal{G}_3 \quad (\text{S54})$$

are the moiré reciprocal unit vectors. We can re-write  $\mathcal{H}1$  in compact form as

$$\mathcal{H}_1 = \frac{1}{N_c} \sum_{\mu} \sum_{n,m} \sum_{\mathbf{k}} 2iK [(\mathbf{k} - n\mathbf{b}_2 - m\mathbf{b}_3) \cdot \nabla f_1(\mathbf{K}_{00})] c_{A,1;nm}^{\dagger,(\mu)}(\mathbf{k}) c_{B,1;nm}^{(\mu)}(\mathbf{k}) + \text{H.c.} \quad (\text{S55})$$

where we introduced valley indices as in

$$c_{A,1}^{\dagger,(\mu)}(\mathbf{K}_{00} + \mathbf{k} - n\mathbf{b}_2 - m\mathbf{b}_3) = c_{A,1;nm}^{\dagger,(\mu)}(\mathbf{k}). \quad (\text{S56})$$

The same steps can be applied to the layer 2 terms, provided that we take into account the shift of the Dirac points w.r.t. those of layer 1, together with a rotation in the Fermi velocities due to the rotation of the Bravais lattice vectors entering the definition of  $f_2$ :

$$\mathcal{H}_2 = \frac{1}{N_c} \sum_{\mu} \sum_{n,m} \sum_{\mathbf{k}} 2iK [(\mathbf{k} - \mathbf{q}_1 - n\mathbf{b}_2 - m\mathbf{b}_3) \cdot \hat{R}(\theta) \nabla f_1(\mathbf{K}_{00})] c_{A,2;nm}^{\dagger,(\mu)}(\mathbf{k}) c_{B,2;nm}^{(\mu)}(\mathbf{k}) + \text{H.c.} \quad (\text{S57})$$

where

$$\mathbf{q}_1 = \mathbf{K}'_{00} - \mathbf{K}_{00} \quad (\text{S58})$$

is the relative shift of the Dirac points of layer 2 and 1 in the first BZ. The matrix  $\hat{R}(\theta)$  is an in-plane rotation by the total relative twist angle  $\theta$ . The valley indices for layer 2 are defined precisely as for layer 1.

## B. Inter-layer interactions in the low-energy limit

We first proceed to decouple the inter-layer interactions in the paramagnetic channel as

$$\mathcal{H}_1 = -\frac{1}{2} \sum_{\mu \neq \nu} \sum_{\alpha, \beta} \sum_{\mathbf{R}, \mathbf{R}'} J(\mathbf{R} + \boldsymbol{\tau}_{\alpha} - \mathbf{R}' - \boldsymbol{\tau}'_{\beta}) \langle c_{\alpha,1}^{(\mu)}(\mathbf{R}) c_{\beta,2}^{(\mu)}(\mathbf{R}') \rangle c_{\alpha,1}^{(\nu)}(\mathbf{R}) c_{\beta,2}^{(\nu)}(\mathbf{R}'). \quad (\text{S59})$$

We introduce the Bloch wave expansions of Eq. S38 and carry out the sums over the Bravais lattice vectors. For our choice of half reciprocal unit cells  $C/2$  and  $C'/2$  (Fig. S1), pairing terms at opposite momenta have vanishing weight and are ignored. For the remaining terms we use

$$\sum_{\mathbf{R}} J(\mathbf{R} + \boldsymbol{\tau}_{\alpha} - \mathbf{R}' - \boldsymbol{\tau}'_{\beta}) e^{i\mathbf{k}\cdot\mathbf{R}} \approx \sum_{\mathbf{G}} e^{-i(\mathbf{k}+\mathbf{G})(\boldsymbol{\tau}_{\alpha} - \mathbf{R}' - \boldsymbol{\tau}'_{\beta})} J(\mathbf{k} + \mathbf{G}) \quad (\text{S60})$$

via the Poisson summation formula, where

$$J(\mathbf{k} + \mathbf{G}) = \frac{1}{a} \int_a d^2r J(\mathbf{r}) e^{i(\mathbf{k}+\mathbf{G})\cdot\mathbf{r}} \quad (\text{S61})$$

is the Fourier transform of  $J$ , defined over the unit cell of layer 1 with an area  $a$ . Also taking into account the conservation of momentum, we obtain

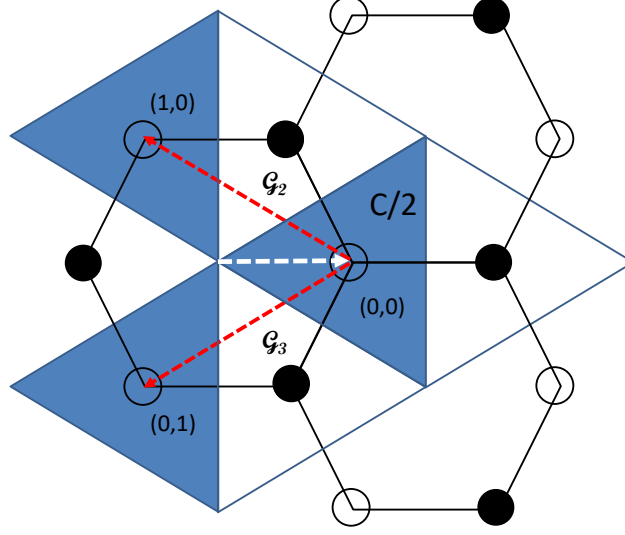


FIG. S1: Extended BZ for layer 1. The blue shaded areas represent our choice of (half) unit cells here, labeled by  $C/2$ . Note that these are equivalent to the unit cell shown in Fig. 3 (d) of the main text. The white vector indicates the position of the Dirac point in the first BZ w.r.t. to the origin, which coincides with the twist axis. The red vectors are the reciprocal unit vectors  $\mathcal{G}_2$  and  $\mathcal{G}_3$ . The pairs of indices label the valleys. A twisted variant of this figure can be drawn for layer 2.

$$\begin{aligned} \mathcal{H}_I = & -\frac{1}{N_c^2} \sum_{\tilde{\mathbf{k}}, \tilde{\mathbf{s}}} \sum_{\mathbf{G}, \mathbf{G}'} \sum_{\mu} \sum_{\alpha, \beta} \left\{ t_I^{(\alpha\beta)}(\tilde{\mathbf{k}} + \mathbf{G}, \tilde{\mathbf{s}}) e^{-i\mathbf{G} \cdot \boldsymbol{\tau}_\alpha} e^{i\mathbf{G}' \cdot \boldsymbol{\tau}'_\beta} c_{\alpha,1}^{\dagger,(\mu)}(\tilde{\mathbf{k}}) c_{\beta,2}^{(\mu)}(\tilde{\mathbf{k}} + \mathbf{G} - \mathbf{G}' - \tilde{\mathbf{s}}) \right. \\ & \left. + t_{II}^{(\alpha\beta)}(\tilde{\mathbf{k}} + \mathbf{G}, \tilde{\mathbf{s}}) e^{-i\mathbf{G} \cdot \boldsymbol{\tau}_\alpha} e^{i\mathbf{G}' \cdot \boldsymbol{\tau}'_\beta} c_{\alpha,1}^{\dagger,(\mu)}(\tilde{\mathbf{k}}) c_{\beta,2}^{(\mu)}(\tilde{\mathbf{k}} + \mathbf{G} - \mathbf{G}' + \tilde{\mathbf{s}}) \right\} + \text{H.c.}, \end{aligned} \quad (\text{S62})$$

where

$$\begin{aligned} t_I^{(\alpha\beta)}(\tilde{\mathbf{k}} + \mathbf{G}, \tilde{\mathbf{s}}) &= \frac{4}{NN_c^2} \sum_{\tilde{\mathbf{k}}_a} J(\tilde{\mathbf{k}} + \mathbf{G} - \tilde{\mathbf{k}}_a) \langle c_{\alpha,1}^{(\nu)}(\tilde{\mathbf{k}}_a) c_{\beta,2}^{\dagger,(\nu)}(\tilde{\mathbf{k}}_a - \tilde{\mathbf{s}}) \rangle \\ t_{II}^{(\alpha\beta)}(\tilde{\mathbf{k}} + \mathbf{G}, \tilde{\mathbf{s}}) &= \frac{4}{NN_c^2} \sum_{\tilde{\mathbf{k}}_a} J(\tilde{\mathbf{k}} + \mathbf{G} + \tilde{\mathbf{k}}_a) \langle c_{\alpha,1}^{\dagger,(\nu)}(\tilde{\mathbf{k}}_a) c_{\beta,2}^{(\nu)}(\tilde{\mathbf{k}}_a - \tilde{\mathbf{s}}) \rangle, \end{aligned} \quad (\text{S63})$$

where we accounted for a mean-field ansatz which preserves the spin  $\text{SO}(3)$  symmetry, implying expectation values which are independent of the flavor indices. Note that the sums over tilde momenta cover the extended BZ.

The form of  $\mathcal{H}_I$  is strongly reminiscent of the inter-layer hybridization in twisted bilayer graphene [S8]. We can show that it reduces to a sum over an extended moiré BZ in the low-energy limit by applying the steps of Sec. V A:

$$\begin{aligned} \mathcal{H}_I \approx & -\frac{1}{N_c} \sum_{\mathbf{k}, \mathbf{s}} \sum_{n', m', n'', m''} \sum_{\mu} \sum_{\alpha, \beta} \left\{ t_{I;n'm',n''m''}^{(\alpha\beta)}(\mathbf{k}, \mathbf{s}) e^{-i((n''-n')\mathcal{G}_2 + (m''-m')\mathcal{G}_3) \cdot (\boldsymbol{\tau}_\alpha - \boldsymbol{\tau}_\beta)} c_{1,\alpha;n'm'}^{\dagger,(\mu)}(\mathbf{k}) c_{2,\beta;n''m''}^{(\mu)}(\mathbf{k} - \mathbf{s}) \right. \\ & \left. + t_{II;n'm',n''m''}^{(\alpha\beta)}(\mathbf{k}, \mathbf{s}) e^{-i((n''-n')\mathcal{G}_2 + (m''-m')\mathcal{G}_3) \cdot (\boldsymbol{\tau}_\alpha - \boldsymbol{\tau}_\beta)} c_{1,\alpha;n'm'}^{\dagger,(\mu)}(\mathbf{k}) c_{2,\beta;n''m''}^{(\mu)}(\mathbf{k} + \mathbf{s}) + \text{H.c.} \right\} \end{aligned} \quad (\text{S64})$$

where

$$\begin{aligned} & t_{I;n'm',n''m''}^{(\alpha\beta)}(\mathbf{k}, \mathbf{s}) \\ &= \frac{4}{N_c N} \sum_{n_a, m_a} \sum_{\mathbf{k}_a} J((n'' - n' - n_a)\mathcal{G}_2 + (m'' - m' - m_a)\mathcal{G}_3) e^{i(n_a\mathcal{G}_2 + m_a\mathcal{G}_3) \cdot (\boldsymbol{\tau}_\alpha - \boldsymbol{\tau}_\beta)} \langle c_{\alpha,1;00}^{(\nu)}(\mathbf{k}_a) c_{\beta,2;n_a m_a}^{\dagger,(\nu)}(\mathbf{k}_a - \mathbf{s}) \rangle \end{aligned} \quad (\text{S65})$$



$$\begin{aligned}
& t_{II;n'm',n''m''}^{(\alpha\beta)}(\mathbf{k}, \mathbf{s}) \\
&= \frac{4}{N_c N} \sum_{n_a, m_a} \sum_{\mathbf{k}_a} J(2\mathbf{K}_{00} + (n'' - n' + n_a)\mathcal{G}_2 + (m'' - m' + m_a)\mathcal{G}_3) e^{-i(n_a\mathcal{G}_2 + m_a\mathcal{G}_3) \cdot (\boldsymbol{\tau}_\alpha - \boldsymbol{\tau}_\beta)} \langle c_{\alpha,1;00}^{\dagger,(\nu)}(\mathbf{k}_a) c_{\beta,2;n_a m_a}^{(\nu)}(\mathbf{k}_a - \mathbf{s}) \rangle
\end{aligned} \tag{S66}$$

These terms represent an effective hybridization between states on layer 1, with Dirac points periodically extended throughout the moiré BZ zone, and all states on layer 2, with Dirac points which are shifted by a fixed vector  $\mathbf{q}_1$  (Eq. S58). This expression is invariant up to a phase under a translation by moiré reciprocal vectors (Eqs. S53, S54). Also note that all sums involve vectors in the vicinity of the pair of Dirac points in the first BZ. In addition, we assumed that the Fourier transform of  $J$  varies slowly on the scale of a single Moire reciprocal unit cell.

We further simplify these expression via the following three assumptions. First, we restrict the intermediate summations over  $n_a, m_a$  to the leading 7 terms corresponding to  $J(0), J(\pm\mathcal{G}_2), J(\pm\mathcal{G}_3), J(\pm\mathcal{G}_2 \mp \mathcal{G}_3)$  for  $t_I$ , and the leading 6 terms corresponding to  $J(2\mathbf{K}_{00}), J(2\mathbf{K}_{00} + 2\mathcal{G}_2), J(2\mathbf{K}_{00} + 2\mathcal{G}_3), J(2\mathbf{K}_{00} + \mathcal{G}_2), J(2\mathbf{K}_{00} + \mathcal{G}_3), J(2\mathbf{K}_{00} + \mathcal{G}_2 + \mathcal{G}_3)$  for  $t_{II}$ . These explicitly preserve a  $C_3$  rotation symmetry. Secondly, we restrict the hybridization to states corresponding to NN Dirac points in the extended moiré zone. For given  $n', m'$ , this is done by imposing

$$n''\mathbf{b}_2 + m''\mathbf{b}_3 + \mathbf{s} = \mathbf{q} + n'\mathbf{b}_2 + m'\mathbf{b}_3 + \begin{cases} 0 \\ \mathbf{b}_2 \\ \mathbf{b}_3 \end{cases} \tag{S67}$$

, with  $\mathbf{q}$  restricted to lie inside a moiré reciprocal unit cell, and by subsequently eliminating the sums over  $n'', m''$  and  $\mathbf{s}$ . States near neighboring Dirac points are expected to provide the leading contributions to the effective hybridization in the low-energy limit. With these assumptions, the only allowed terms for fixed  $\mathbf{q}$  are

$$\begin{aligned}
t_{I;n'm',n'm'}^{(\alpha\beta)}(\mathbf{k}, \mathbf{q}) &= \frac{4}{N} \sum_{\mathbf{k}_a} \left\{ J(0) \langle c_{\alpha,1;00}^{(\nu)}(\mathbf{k}_a) c_{\beta,2;00}^{\dagger,(\nu)}(\mathbf{k}_a - \mathbf{q}) \rangle + J(-\mathcal{G}_2) e^{i\mathcal{G}_2(\boldsymbol{\tau}_\alpha - \boldsymbol{\tau}_\beta)} \langle c_{\alpha,1;00}^{(\nu)}(\mathbf{k}_a) c_{\beta,2;10}^{\dagger,(\nu)}(\mathbf{k}_a - \mathbf{q}) \rangle \right. \\
&\quad \left. + J(-\mathcal{G}_3) e^{i\mathcal{G}_3(\boldsymbol{\tau}_\alpha - \boldsymbol{\tau}_\beta)} \langle c_{\alpha,1;00}^{(\nu)}(\mathbf{k}_a) c_{\beta,2;01}^{\dagger,(\nu)}(\mathbf{k}_a - \mathbf{q}) \rangle \right\}
\end{aligned} \tag{S68}$$

$$\begin{aligned}
t_{I;n'm',n'+1m'}^{(\alpha\beta)}(\mathbf{k}, \mathbf{q}) &= \frac{4}{N} \sum_{\mathbf{k}_a} \left\{ J(0) \langle c_{\alpha,1;00}^{(\nu)}(\mathbf{k}_a) c_{\beta,2;10}^{\dagger,(\nu)}(\mathbf{k}_a - \mathbf{q}) \rangle + J(\mathcal{G}_2) e^{-i\mathcal{G}_2(\boldsymbol{\tau}_\alpha - \boldsymbol{\tau}_\beta)} \langle c_{\alpha,1;00}^{(\nu)}(\mathbf{k}_a) c_{\beta,2;00}^{\dagger,(\nu)}(\mathbf{k}_a - \mathbf{q}) \rangle \right. \\
&\quad \left. + J(\mathcal{G}_2 - \mathcal{G}_3) e^{-i(\mathcal{G}_2 - \mathcal{G}_3) \cdot (\boldsymbol{\tau}_\alpha - \boldsymbol{\tau}_\beta)} \langle c_{\alpha,1;00}^{(\nu)}(\mathbf{k}_a) c_{\beta,2;01}^{\dagger,(\nu)}(\mathbf{k}_a - \mathbf{q}) \rangle \right\}
\end{aligned} \tag{S69}$$

$$\begin{aligned}
t_{I;n'm',n'm'+1}^{(\alpha\beta)}(\mathbf{k}, \mathbf{q}) &= \frac{4}{N} \sum_{\mathbf{k}_a} \left\{ J(0) \langle c_{\alpha,1;00}^{(\nu)}(\mathbf{k}_a) c_{\beta,2;01}^{\dagger,(\nu)}(\mathbf{k}_a - \mathbf{q}) \rangle + J(\mathcal{G}_3) e^{-i\mathcal{G}_3 \cdot (\boldsymbol{\tau}_\alpha - \boldsymbol{\tau}_\beta)} \langle c_{\alpha,1;00}^{(\nu)}(\mathbf{k}_a) c_{\beta,2;00}^{\dagger,(\nu)}(\mathbf{k}_a - \mathbf{q}) \rangle \right. \\
&\quad \left. + J(-\mathcal{G}_2 + \mathcal{G}_3) e^{i(\mathcal{G}_2 - \mathcal{G}_3) \cdot (\boldsymbol{\tau}_\alpha - \boldsymbol{\tau}_\beta)} \langle c_{\alpha,1;00}^{(\nu)}(\mathbf{k}_a) c_{\beta,2;10}^{\dagger,(\nu)}(\mathbf{k}_a - \mathbf{q}) \rangle \right\}
\end{aligned} \tag{S70}$$

$$\begin{aligned}
t_{II;n'm',n'm'}^{(\alpha\beta)}(\mathbf{k}, \mathbf{q}) &= \frac{4}{N} \sum_{\mathbf{k}_a} \left\{ J(2\mathbf{K}_{00}) \langle c_{\alpha,1;00}^{\dagger,(\nu)}(\mathbf{k}_a) c_{\beta,2;00}^{(\nu)}(\mathbf{k}_a - \mathbf{q}) \rangle \right. \\
&\quad + J(2\mathbf{K}_{00} + \mathcal{G}_2) e^{-i\mathcal{G}_2 \cdot (\boldsymbol{\tau}_\alpha - \boldsymbol{\tau}_\beta)} \langle c_{\alpha,1;00}^{\dagger,(\nu)}(\mathbf{k}_a) c_{\beta,2;10}^{\dagger,(\nu)}(\mathbf{k}_a - \mathbf{q}) \rangle \\
&\quad \left. + J(2\mathbf{K}_{00} + \mathcal{G}_3) e^{-i\mathcal{G}_3 \cdot (\boldsymbol{\tau}_\alpha - \boldsymbol{\tau}_\beta)} \langle c_{\alpha,1;00}^{\dagger,(\nu)}(\mathbf{k}_a) c_{\beta,2;01}^{\dagger,(\nu)}(\mathbf{k}_a - \mathbf{q}) \rangle \right\}
\end{aligned} \tag{S71}$$

$$\begin{aligned}
t_{II;n'm',n'+1m'}^{(\alpha\beta)}(\mathbf{k}, \mathbf{q}) &= \frac{4}{N} \sum_{\mathbf{k}_a} \left\{ J(2\mathbf{K}_{00} + 2\mathcal{G}_2) e^{-2i\mathcal{G}_2 \cdot (\boldsymbol{\tau}_\alpha - \boldsymbol{\tau}_\beta)} \langle c_{\alpha,1;00}^{\dagger,(\nu)}(\mathbf{k}_a) c_{\beta,2;10}^{(\nu)}(\mathbf{k}_a - \mathbf{q}) \rangle \right. \\
&\quad + J(2\mathbf{K}_{00} + \mathcal{G}_2) e^{-i\mathcal{G}_2 \cdot (\boldsymbol{\tau}_\alpha - \boldsymbol{\tau}_\beta)} \langle c_{\alpha,1;00}^{\dagger,(\nu)}(\mathbf{k}_a) c_{\beta,2;00}^{\dagger,(\nu)}(\mathbf{k}_a - \mathbf{q}) \rangle \\
&\quad \left. + J(2\mathbf{K}_{00} + \mathcal{G}_2 + \mathcal{G}_3) e^{-i(\mathcal{G}_2 + \mathcal{G}_3) \cdot (\boldsymbol{\tau}_\alpha - \boldsymbol{\tau}_\beta)} \langle c_{\alpha,1;00}^{(\nu)}(\mathbf{k}_a) c_{\beta,2;01}^{\dagger,(\nu)}(\mathbf{k}_a - \mathbf{q}) \rangle \right\}
\end{aligned} \tag{S72}$$

$$\begin{aligned}
t_{II;n'm',n'm'+1}^{(\alpha\beta)}(\mathbf{k}, \mathbf{q}) = & \frac{4}{N} \sum_{\mathbf{k}_a} \left\{ J(2\mathbf{K}_{00} + 2\mathbf{g}_3) e^{-2i\mathbf{g}_3 \cdot (\boldsymbol{\tau}_\alpha - \boldsymbol{\tau}_\beta)} \langle c_{\alpha,1;00}^{\dagger,(\nu)}(\mathbf{k}_a) c_{\beta,2;01}^{(\nu)}(\mathbf{k}_a - \mathbf{q}) \rangle \right. \\
& + J(2\mathbf{K}_{00} + \mathbf{g}_3) e^{-i\mathbf{g}_3 \cdot (\boldsymbol{\tau}_\alpha - \boldsymbol{\tau}_\beta)} \langle c_{\alpha,1;00}^{\dagger,(\nu)}(\mathbf{k}_a) c_{\beta,2;00}^{\dagger,(\nu)}(\mathbf{k}_a - \mathbf{q}) \rangle \\
& \left. + J(2\mathbf{K}_{00} + \mathbf{g}_2 + \mathbf{g}_3) e^{-i(\mathbf{g}_2 + \mathbf{g}_3) \cdot (\boldsymbol{\tau}_\alpha - \boldsymbol{\tau}_\beta)} \langle c_{\alpha,1;00}^{(\nu)}(\mathbf{k}_a) c_{\beta,2;10}^{\dagger,(\nu)}(\mathbf{k}_a - \mathbf{q}) \rangle \right\} \quad (S73)
\end{aligned}$$

Finally, these expressions simplify considerably once we ignore the relative variation of the different  $J$ 's, and we recover the form discussed in the main text.

- 
- [S1] B. S. Shastry and D. Sen, Phys. Rev. B **55**, 2988 (1997), URL <https://link.aps.org/doi/10.1103/PhysRevB.55.2988>.  
[S2] R. R. Biswas, L. Fu, C. R. Laumann, and S. Sachdev, Phys. Rev. B **83**, 245131 (2011), URL <https://link.aps.org/doi/10.1103/PhysRevB.83.245131>.  
[S3] F. L. Pedrocchi, S. Chesi, and D. Loss, Phys. Rev. B **84**, 165414 (2011), URL <https://link.aps.org/doi/10.1103/PhysRevB.84.165414>.  
[S4] S. Chulliparambil, U. F. P. Seifert, M. Vojta, L. Janssen, and H.-H. Tu, Phys. Rev. B **102**, 201111 (2020), URL <https://link.aps.org/doi/10.1103/PhysRevB.102.201111>.  
[S5] E. Fradkin and S. H. Shenker, Phys. Rev. D **19**, 3682 (1979), URL <https://link.aps.org/doi/10.1103/PhysRevD.19.3682>.  
[S6] A. M. Tsvelik and P. Coleman, arXiv:2112.07781 (2021), URL <https://arxiv.org/abs/2112.07781>.  
[S7] H. Yao and D.-H. Lee, Phys. Rev. Lett. **107**, 087205 (2011), URL <https://link.aps.org/doi/10.1103/PhysRevLett.107.087205>.  
[S8] R. Bistritzer and A. H. MacDonald, Proceedings of the National Academy of Sciences **108**, 12233 (2011), URL <https://www.pnas.org/content/108/30/12233>.